

Spectroscopic Abundances and Membership in the Wolf 630 Moving Group

Eric J. Bubar

*Department of Physics and Astronomy, University of Rochester, P.O. Box 270171,
Rochester, NY 14627-0171*

ebubar@gmail.com

Jeremy R. King

Department of Physics and Astronomy, Clemson University, Clemson, SC 29630-0978

jking2@ces.clemson.edu

ABSTRACT

The concept of kinematic assemblages evolving from dispersed stellar clusters has remained contentious since Eggen's initial formulation of moving groups in the 1960's. With high quality parallaxes from the Hipparcos space astrometry mission, distance measurements for thousands of nearby, seemingly isolated stars are currently available. With these distances, a high resolution spectroscopic abundance analysis can be brought to bear on the alleged members of these moving groups. If a structure is a relic of an open cluster, the members can be expected to be monolithic in age and abundance inasmuch as homogeneity is observed in young open clusters. In this work we have examined 34 putative members of the proposed Wolf 630 moving group using high resolution stellar spectroscopy. The stars of the sample have been chemically tagged to determine abundance homogeneity and confirm the existence of a homogeneous subsample of 19 stars. Fitting the homogeneous subsample with Yale-Yonsei isochrones yields a single evolutionary sequence of $\sim 2.7 \pm 0.5$ Gyr. It is concluded that this 19 star subsample of the Wolf 630 moving group sample of 34 stars could represent a dispersed cluster with an $\langle [\text{Fe}/\text{H}] \rangle = -0.01 \pm 0.02$ and an age of 2.7 ± 0.5 Gyr. In addition, chemical abundances of Na and Al in giants are examined for indications of enhancements as observed in field giants of old open clusters, overexcitation/ionization effects are explored in the cooler dwarfs of the sample and oxygen is derived from the infrared triplet and the forbidden line at $\lambda 6300$ Å.

Subject headings: stars: abundances - stars: kinematics and dynamics - stars: late-type

1. INTRODUCTION

A major goal of modern astronomy is to piece together the dynamic and chemical evolution of the Galactic disk. To this end, one of the principle approaches for probing the disk has been to study open clusters. Clusters are valuable astrophysical tools as they share common distances, common ages and common initial chemical abundances. With the disk richly populated by both field stars and open clusters, and considering that clusters are relatively well studied, the logical step in piecing together a more complete picture of the chemical and dynamical history of the disk is to study field stars.

In recent years, the advent of large surveys such as *HIPPARCOS* (Perryman & ESA 1997) has yielded precise parallaxes for thousands of nearby field stars, and in doing so, provided the necessary tools for investigating the field. In particular, studies of the velocity distributions of disk field stars in the solar neighborhood have identified stellar overdensities in kinematic phase space (Skuljan et al. (1999)). The potential application of these velocity structures, commonly referred to as moving groups, was first identified by Eggen (1958) who considered these assemblages to be relic structures of dissolved open clusters. In this paradigm, a moving group is essentially a spatially unassociated open cluster; therefore it should possess some of the same characteristics that make open clusters such valuable astrophysical tools (common ages and common initial chemical abundances) and similar techniques that are useful for studying open clusters could be applied.

Relatively little work has been done to explore the reality of smaller moving groups (kinematic assemblages of ~ 100 stars) as dissolved open clusters and their use in chemically tagging the galactic disk, with two notable exceptions: the Ursa Major Group and the HR1614 Moving Group. Soderblom & Mayor (1993) examined the Ursa Major moving group and utilized age information inferred from chromospheric emission to constrain group membership in UMa. While this study did not utilize chemical tagging to constrain group membership, it did illustrate the viability of moving groups as dissolved populations of open clusters. King et al. (2003) and King & Schuler (2005) revisited the membership of the UMa group, using new and extant abundances. They used the results to constrain membership in the UMa group, showed the members to be chemically homogeneous, and noticed overexcitation/overionization effects in the cooler field star members of the group, similar to those observed in young (< 500 Myr) cool open cluster dwarfs (Schuler et al. (2003), Schuler et al. (2004)). The first in depth application of chemical tagging to constrain moving group membership was by De Silva et al. (2007), who derived abundances for various elements for the HR 1614 moving group. They found that for their 18 star sample, 14 stars were metal-rich ($[\text{Fe}/\text{H}] \geq 0.25$ dex with $\sigma=0.03$) leading to the conclusion that the HR 1614 moving group, with its distinct kinematics and distinctly super-solar chemical abundances, was a remnant

of a dissolved open cluster.

In the field of moving group populations, the classical Wolf 630 moving group is an intriguing target. The first identification of the Wolf 630 moving group was made by Eggen (1965) who noted that several K and M dwarfs and giants in the solar neighborhood appeared to have similar space motions to that of the multiple star system Wolf 630 ((U,V,W)=(23, -33, 18) kms^{-1}). These kinematics, distinctive of membership in an old disk population, placed the stars in a relatively sparsely populated region of kinematic phase space (Eggen 1969). Eggen also noted that the color magnitude diagram for the K and M dwarfs and giants with kinematics similar to those of Wolf 630 appeared to trace an evolutionary sequence similar to the old (~ 5 Gyr; Jones et al. (1999)) M67 open cluster. Although his sources are not completely transparent, at least some (17 of 54 stars) of the distances in his study were determined from trigonometric parallaxes, with the remainder coming from “luminosity estimates of many kinds”. As a rudimentary form of chemical tagging, Eggen (1970) estimated metallicities of 23 Wolf 630 group members through *uvby*- β photometry. Variations in the $\delta[m_1]$ index were found to be comparable to the Hyades, Praesepe, and the Coma Berenices clusters, implying chemical homogeneity.

Tuominen & Vilhu (1979) studied the chemical composition of five field giant stars that were alleged members of Wolf 630 using high dispersion coude spectra described in Tuominen & Vilhu (1979). Employing a curve of growth approach and measured equivalent widths, they found that three stars appeared to be chemically homogeneous with an overall metallicity for Wolf 630 of $[\text{Fe}/\text{H}] \sim +0.23$. However, it must be noted that their abundances were not measured with respect to the Sun, but are instead quoted with respect to a standard star of presumed solar metallicity (HD 197989), which has since been determined to be a K0III. While they derived a metallicity of 0.00 for their reference star, literature determinations suggest a value of -0.24. This would lower the average metallicity for the group to $[\text{Fe}/\text{H}] \sim -0.02$.

McDonald & Hearnshaw (1983) revisited the membership of the Wolf 630 moving group by recreating the approach presumably utilized by Eggen (1965) to find his original Wolf sample. In summary, they calculate the parallax that yields a V velocity for each group candidate equal to the assumed group velocity of $V = -32.8 \pm 1.3 \text{ kms}^{-1}$. The final absolute magnitudes they report assume these parallaxes. Typical uncertainties in their absolute magnitudes appear to be between 0.2-0.4 magnitudes, larger than magnitude uncertainties obtainable with precise parallax information currently available from Hipparcos. The color-magnitude diagram assuming these M_V values was compared to the scatter of apparent members with the observed scatter in the old open cluster M67. They concluded that either (1) the intrinsic scatter in the Wolf 630 moving group color-magnitude diagram was greater

than that of M67, or (2) the errors in radial velocities and/or proper motions they utilized must have been underestimated by a factor of 2.4 or (3) many of the stars in their sample were, in fact, non-members.

Taylor (1994) examined metallicities from “published values of $[\text{Fe}/\text{H}]$ from diverse papers” of 40 members of the Wolf 630 group. His sample contains 26 % of Eggen’s original objects (Eggen 1969). He concluded that metallicity dispersions within his sample were too great for meaningful conclusions about the existence or non-existence of a genuine, chemically distinct Wolf 630 moving group. This suggests the need to obtain high quality $[\text{Fe}/\text{H}]$ determinations with minimal uncertainties in testing for chemical uniqueness in a putative Wolf 630 sample.

The analysis of solar neighborhood Hipparcos data by Skuljan et al. (1999) indicates a kinematic rediscovery of the Wolf 630 group. Their figure 10, showing the UV velocity distribution for 3561 late type dwarfs in the solar neighborhood presents a clear overdensity of stars near the position of Wolf 630. Furthermore, this structure appears to be distinctly separated from any other known moving groups or stellar streams. This provides compelling evidence that Wolf 630 is a real kinematic structure. The question to be asked is if this kinematic structure is composed of stars with a common origin?

Despite the distinctive kinematics exhibited by the Wolf 630 moving group when examined with updated Hipparcos parallaxes, it has not been specifically targeted in an abundance study which makes use of the modern astrometric and spectroscopic data. This is remedied in this paper, where accurate parallaxes and photometry from the updated *HIPPARCOS* data reduction (van Leeuwen 2007) coupled with high precision radial velocities from CORAVEL (Nordström et al. (2004) and references therein) allow for developing a Wolf 630 sample with internally consistent distances and absolute magnitudes, thereby removing the uncertainties faced by McDonald & Hearnshaw (1983). Furthermore, our uniform high resolution spectroscopic study of Wolf 630 moving group candidate members provides a single, consistent set of metallicities with low internal uncertainty to test chemical homogeneity in the group, removing the largest source of uncertainty from Taylor (1994).

2. DATA, OBSERVATIONS AND ANALYSIS

2.1. Literature Data

The 34 stars in this sample, listed in Table 1, were previously identified as members of the Wolf 630 group (Eggen (1969), McDonald & Hearnshaw (1983)) according to their UVW kinematics. In this study, we use updated parallaxes and proper motions from the latest

reduction of Hipparcos data (van Leeuwen 2007). Precision radial velocities were taken from the compilation of Nordström et al. (2004). Visible band photometry (B , V , B_{Tycho} , V_{Tycho}) was taken from the *HIPPARCOS* catalogue (Perryman & ESA 1997). Near infrared J , H and K photometry was taken from the 2MASS Catalog (Cutri et al. 2003).

2.2. Kinematics

We determined galactic UVW kinematics from the proper motions, parallaxes and radial velocities using a modified version of the code of Johnson & Soderblom (1987). Here, the U velocity is positive towards the Galactic center, the V velocity is positive in the direction of Galactic rotation and the W velocity is positive in the direction of the North Galactic Pole (NGP). The relevant parameters for determination of these kinematics are presented in Table 1.

2.3. Spectroscopic Observations and Reductions

Spectroscopy of the sample was obtained in March 2007 and November 2008 with the KPNO 4 meter Mayall telescope, the echelle spectrograph with grating 58.5-63 and a T2KB 2048X2048 CCD detector. The slit width of ~ 1 arcsec yielded a resolution of $R \sim 40,000$ with a typical S/N of 200 per summed pixel. The spectra have incomplete wavelength coverage extending from approximately 5800 Å to 7800 Å. The spectra have been reduced using standard routines in the *echelle* package of IRAF¹. These include bias correction, flat-fielding, scattered light correction, order extraction, and wavelength calibration. Sample spectra are presented in Figure 1.

2.4. Line Selection

Spectroscopic physical parameters are typically determined by enforcing balance constraints on abundances derived from lines of Fe, which has a plethora of suitable neutral (Fe I) and ionized (Fe II) features in the optical. We compiled low excitation potential ($\chi < 6.00$ eV) Fe I and Fe II lines from Thevenin (1990), the VIENNA Atomic Line

¹IRAF is distributed by the National Optical Astronomy Observatories, which are operated by the Association of Universities for Research in Astronomy, Inc., under cooperative agreement with the National Science Foundation.

Database (Piskunov et al. (1995), Ryabchikova et al. (1997), Kupka & Ryabchikova (1999), Kupka et al. (2000)), Yong et al. (2004), Schuler et al. (2006) and De Silva et al. (2007). Lines that were not apparent in a high-resolution solar spectrum (Kurucz 2005) were removed from the linelist. In order to guarantee that these lines were unaffected by blending effects, especially those arising in cool stars that might not be noticeable in the solar spectrum, the 2002 version of the MOOG spectral analysis program (Sneden 1973) was used to compute synthetic spectra in 1 Å blocks surrounding all Fe features, using VALD linelists. If a line had closely neighboring features with MOOG-based relative strength parameters within an order of magnitude it was removed from consideration. In this manner, a final list of 145 Fe I lines and 11 Fe II lines was formed. These linelists are presented in Table 2. The equivalent widths listed are for measurements in a high resolution solar spectrum.

Linelists for other elements of interest have also been compiled from multiple sources (Thevenin (1990), King et al. (1998), De Silva et al. (2006)). These elements include Li, Na, Al, Ba, a selection of α elements (O, Mg, Si, Ca, Ti I and Ti II) and a selection of Fe peak elements (Cr, Mn and Ni). The lines are also given in Table 2. Equivalent widths are again for measurements in the high resolution solar spectrum. The equivalent widths that were measurable for each individual star are given in Table 4, with corresponding abundances derived from each equivalent width.

2.5. Equivalent Widths

Equivalent widths for the lines of interest were measured in each star and in a high resolution solar spectrum using the spectral analysis tool SPECTRE (Fitzpatrick & Sneden 1987). Final abundances were obtained from equivalent widths through use of the MOOG LTE spectral analysis tool (Sneden 1973) with an input Kurucz model atmosphere characterized by the four fundamental physical parameters: temperature, surface gravity, microturbulent velocity (ζ) and metallicity. Unless noted otherwise all abundances are differential with respect to the Sun and are presented in the standard bracket notation ($[X/H] = \log(\frac{N(X)}{N(H)})_* - \log(\frac{N(X)}{N(H)})_\odot$ where $\log N(H) \equiv 12$).

2.6. Initial Parameters: Photometric

The color- T_{eff} - $[\text{Fe}/\text{H}]$ calibrations of Ramírez & Meléndez (2005) were used to determine photometric temperatures from Johnson $B - V$, Tycho $B_T - V_T$, Johnson/2MASS $V - J_2$, $V - H_2$ and $V - K_2$. The color indices for 8 stars were outside of the calibrated ranges;

consequently photometric temperatures were not derived. Uncertainties in the photometric temperatures were conservatively taken as the standard deviation of the temperatures derived from each of the respective colors. With the availability of high quality Hipparcos Parallaxes, physical surface gravities were calculated from:

$$\log \frac{g}{g_{\odot}} = \log \frac{M}{M_{\odot}} + 4 \log \frac{T_{eff}}{T_{eff,\odot}} + 0.4V_o + 0.4B.C. + 2 \log \pi + 0.12$$

where M is the mass in solar masses, estimated from Yale-Yonsei isochrones (Demarque et al. 2004) of solar metallicity, bolometric corrections are from Gray (2005), and π is the parallax. Initial microturbulent velocities were found from the calibrations of Allende Prieto et al. (2004). These photometric parameters provided the initial guesses for physical parameters when deriving the final spectroscopic values. Additionally, the photometric calibrations provided reasonable estimates to compare to spectroscopically derived results. Using the updated calibrations of Casagrande et al. (2010) does not change the results described herein.

2.7. Spectroscopic Parameters

The refined Fe linelists discussed above acted as target lists for each of the stars in the sample. The typical star contained ~ 80 of the 145 good Fe I lines that were measurable in the solar spectrum. Several of the stars showed correlations between Fe I excitation potential and reduced equivalent width. If ignored, such correlations can be imposed onto the temperatures and microturbulent velocities, resulting in non-unique solutions of physical parameters. Consequently, two linelists for the Fe I lines were formed for each star; a correlated and an uncorrelated sample. Final basic physical parameters for the sample were derived using a modification to the standard techniques of Fe excitation/ionization/line strength balance. In all the approaches described below, a differential analysis was used where the same lines were measured in a solar spectrum and in the stellar spectra. Final abundances were then determined by subtracting the solar abundance from the stellar abundance in a line by line fashion.

The first technique utilized the uncorrelated line sample and proceeded as follows: temperatures of input model atmospheres were adjusted to remove any correlation in solar-normalized abundances with respect to excitation potential; ζ is adjusted to remove any correlation with line strength and $\log g$ is adjusted until the mean abundance from Fe II lines matches the abundance from Fe I lines. This approach required simultaneously adjusting temperatures, surface gravities, metallicities and microturbulent velocities to converge to a common solution. Use of the uncorrelated line sample, as described above, is necessary to ensure a unique solution. This approach will be referred to as the “classical” approach.

The second approach used the correlated line sample and the Hipparcos-based physical surface gravities. The Fe II abundances are primarily set by this gravity. The temperature was adjusted to force the mean abundance from Fe I lines to match that from Fe II lines. The microturbulent velocity was adjusted until the abundance from Fe I lines had no dependence on reduced equivalent width. The advantage of this approach is that it does not require simultaneous solutions requiring excitation balance and equivalent width balance, allowing use of a full correlated line sample. This approach will be referred to as the “physical surface gravity” approach.

When comparing results from the classical and physical surface gravity approaches it was apparent that the microturbulent velocities were nearly identical ($\delta\zeta \approx \pm 0.04 \text{ km s}^{-1}$). Thus our final spectroscopic parameters were determined as follows. The microturbulent velocities from the “classical” approach and the “physical surface gravity” approach were averaged to yield a final value. The correlated line sample was used to determine the temperature and surface gravity using excitation/ionization balance. For the remainder of the work, the results from this approach were used for the physical parameters of these 30 stars. The remaining 4 stars would not converge to an acceptable solution and the following alternative approach was developed.

The coolest stars in the sample (HIP105341-dwarf, HIP114155-giant and HIP5027-dwarf) had an insufficient number of well-measured Fe II lines for accurately determining the surface gravity spectroscopically. Consequently, Hipparcos-based physical surface gravities were used to set the gravity, and the temperature and microturbulence were iterated to eliminate correlations in $[\text{Fe I}/\text{H}]$ versus excitation potential and versus the reduced equivalent width. This is the “physical surface gravity” approach.

Finally, one of the stars in the sample (HIP 5027) had a microturbulence correlation which could not be removed without utilizing unreasonable surface gravities. For this star, the surface gravity was set based on Yale-Yonsei isochrones (Demarque et al. 2004). The microturbulent velocity was set to zero and the temperature was determined from excitation balance.

The final basic physical parameters (T_{Spec} , $\log g$, microturbulent velocity (ξ) and $[\text{Fe}/\text{H}]$) are presented in Table 3 and final abundances are summarized in Table 5. For the interested reader, we also provide plots of all abundances ($[\text{X}/\text{H}]$) versus $[\text{Fe}/\text{H}]$ in an appendix.

2.8. Lithium

Abundances have been derived for lithium using spectral synthesis. We use the `synth` driver of MOOG to synthesize a spectrum of the lithium line at $\lambda=6707.79$ Å with an updated version of the linelist from King et al. (1997). Appropriate smoothing factors were determined by measuring clean, weak lines in the lithium region. The lithium abundance was varied until a best fit is obtained from visual inspection. A sample synthesis is presented in Figure 5.

Uncertainties in lithium abundances have been determined by examining the change in Li abundance in syntheses with arbitrary changes in physical parameters of $\Delta T=150$ K, $\Delta \log g=0.12$ cm s⁻² and $\Delta \xi=0.60$ km s⁻¹, and adding the resultant abundance differences in quadrature.

2.9. Oxygen

Oxygen abundances for many stars have been derived from the near-IR $\lambda 7771$ equivalent widths. Abundances derived from the triplet are known to be enhanced by NLTE effects; therefore appropriate corrections have been applied following Takeda (2003).

For the giants and subgiants, oxygen abundances have also been derived from the forbidden line at $\lambda 6300.34$ Å. While this line is found to be free from NLTE effects (Takeda (2003)), care must be taken as the line is blended with a nearby Ni feature at $\lambda 6300.31$ Å. This blend is treated using the `blends` driver of MOOG, following Schuler et al. (2006). The Ni abundance utilized to account for blending is the mean value derived from the EWs of Ni I lines in our sample.

A possible CN feature at 6300.265 Å and two at 6300.482 Å with $\log(gf)$ values of -2.70, -2.24 and -2.17 are claimed by Davis & Phillips (1963). In order to explore these blends, multiple syntheses of the $\lambda 6300$ Å region were performed using high resolution spectral atlases of the Sun (Kurucz 2005) and the K giant, Arcturus (Hinkle et al. 2000). The CN features, if real, were found to be unimportant in the solar spectrum. Large variations in carbon abundances (> 0.50 dex) appear to have little impact on the overall spectrum. For warm dwarfs, the syntheses confirm that the Ni features are the dominant blends affecting O determination.

The situation appears to be dramatically different for cooler giants. In the high resolution spectral atlas for Arcturus, the CN blend, if real, appears to dominate over the Nickel blend. Oxygen syntheses were performed in order to calibrate the gf values of the CN

molecules in the linelist to match the spectrum of Arcturus, but results were inconclusive. In particular, appropriate smoothing factors were difficult to determine as the ultra high resolution of the Arcturus atlas makes Gaussian smoothing by an instrumental profile inappropriate. In an attempt to accurately reflect the smoothing in the spectral atlas, broadening was done using a convolution of a macroturbulent broadening of $5.21 \pm 0.2 \text{ km s}^{-1}$ (Gray 1981) and a rotational broadening characterized by $v \sin(i) = 2.4 \pm 0.4 \text{ km s}^{-1}$ (Gray 1981) with a limb darkening coefficient of 0.9 (from Gray (2005)). With this smoothing, the spectrum for Arcturus in the forbidden oxygen region was fit by increasing the CN features gf values by ~ 0.40 dex, while assuming a $[\text{C}/\text{Fe}] = -0.06$ as found by Smith et al. (2002). In attempting to apply this calibrated linelist to synthesize the forbidden line region for one of the giants in our sample (HIP17792; chosen because its physical parameters were similar to those of Arcturus) no reasonable abundance of carbon yielded a satisfactory fit. This may suggest that the gf values in the linelist need to be more well constrained. In light of the ambiguous results, it is concluded that an accurate determination of the carbon abundance is essential for proper treatment of any CN blending feature that may exist. We suggest that a spectroscopic analysis of cool giants with appropriate wavelength coverage to allow measurement of a precise carbon abundance would allow for calibration of the forbidden oxygen linelist, which would be a project of not insignificant interest. Unfortunately the wavelength coverage of the observed spectra does not include any appropriate carbon features to allow definitive conclusions as to the reality of the CN blending features found in Davis & Phillips (1963). In light of the unresolved nature of this CN blending, abundances reported herein do not include it. Further justification for ignoring the CN blending is discussed in the results.

2.9.1. *Uncertainty Estimates*

The uncertainties in experimental and theoretical $\log(gf)$ values (likely at least 0.1 dex) can be a significant source of error; however, by performing a line-by-line differential analysis with respect to the Sun, uncertainties due to transition probabilities are eliminated to first order.

Here, then, it is the uncertainty in physical parameters that underlie the uncertainties in the abundances. Errors in the temperature were determined by adjusting the temperature solution until the correlation between $[\text{Fe}/\text{H}]$ and excitation potential (excitation balance) reached a $1\text{-}\sigma$ linear correlation coefficient for the given number of lines. The uncertainty in microturbulent velocity was determined in the same manner, by adjusting the microturbulence until the linear correlation coefficient for $[\text{Fe}/\text{H}]$ versus equivalent width (equivalent width balance) resulted in a $1\text{-}\sigma$ deviation. For HIP 5027, which would not converge to a

unique solution for microturbulence, an uncertainty in microturbulence of 0.20 km s^{-1} was adopted.

For the cases where the physical surface gravity was utilized, the uncertainty was estimated by propagating the uncertainties in the temperature, mass, apparent magnitude, parallax and bolometric corrections. The uncertainties in the spectroscopically determined surface gravities required a deeper treatment. Since gravity is calculated by eliminating the difference in iron abundance derived from $[\text{Fe I}/\text{H}]$ and $[\text{Fe II}/\text{H}]$, the uncertainty in surface gravity is related to the quadratic sum of the the uncertainties in $[\text{Fe I}/\text{H}]$ and $[\text{Fe II}/\text{H}]$. These abundances, in turn, have sensitivities that depend on the basic physical parameters. Proper uncertainty calculations, therefore, require an iterative procedure. The errors in $[\text{Fe I}/\text{H}]$ and $[\text{Fe II}/\text{H}]$ are a combination of the measurement uncertainties and the uncertainties in the physical parameters. The line measurement uncertainties in Fe I and Fe II were estimated as the standard deviation of the abundances from all Fe I and Fe II lines, respectively. Abundance sensitivities for arbitrary changes in temperature ($\pm 150 \text{ K}$), surface gravity ($\pm 0.12 \text{ dex}$) and microturbulence ($\pm 0.60 \text{ km s}^{-1}$) were determined by adjusting each parameter individually and recording the resultant difference in abundance. To determine abundance uncertainties the abundance differences must be properly normalized by the respective parameter’s uncertainty. For example, in HIP3455 the total temperature uncertainty was found to be 35 K . The final abundance uncertainty introduced by the arbitrary temperature change would, therefore, be equal to the difference in abundance multiplied by $\frac{35\text{K}}{150\text{K}}$, where 35 K is the temperature uncertainty and 150 K is the arbitrary temperature change introduced to determine the temperature sensitivity. For the first calculation the uncertainties in temperature and microturbulent velocity were determined as above and the uncertainty in surface gravity was unknown; consequently its contribution to abundance uncertainty was initially ignored. Adding the measurement errors in $[\text{Fe I}/\text{H}]$ and $[\text{Fe II}/\text{H}]$ in quadrature with the physical parameter abundance uncertainties from temperature and microturbulence yields a first estimate for the uncertainty in the surface gravity. This gravity uncertainty can then be added in quadrature to the line measurement uncertainty, the temperature uncertainty and the microturbulent uncertainty to yield a final uncertainty for the surface gravity. The surface gravity in the model atmosphere was adjusted until the difference in abundance between $[\text{Fe I}/\text{H}]$ and $[\text{Fe II}/\text{H}]$ was equal to their quadrature added uncertainties. The difference between this gravity and the spectroscopically derived gravity provides the final uncertainty in surface gravity.

Uncertainties in abundances were found by introducing arbitrary changes in T , microturbulence and surface gravity ($\Delta T=150 \text{ K}$, $\Delta \xi=0.60 \text{ km s}^{-1}$, and $\Delta \log g=0.12 \text{ cm s}^{-2}$), normalized by the respective parameter uncertainties. The uncertainties introduced by each of these parameter changes was added in quadrature to obtain total parameter-based uncer-

tainties. Measurement uncertainties were taken as the uncertainty in the weighted mean for all lines of a given element. For elements with only a single line available, the standard deviation of all Fe I abundances was utilized as an estimate of the line measurement uncertainty. The final uncertainties in the abundances were determined by adding the parameter-based abundance uncertainties with the measurement uncertainties in quadrature.

A sample table of the normalized parameter changes and their final resultant [Fe I/H] errors on a given star is presented in Table 6.

2.10. Physical Parameter Comparisons:

2.10.1. *Temperatures: Spectroscopic Versus Photometric*

The temperatures for the stars in the sample were determined from photometric calibrations as well as through spectroscopic excitation balance. In Figure 2 the spectroscopic temperature is plotted versus the photometric temperature. The line represents perfect agreement between the two temperatures. It can clearly be seen that the temperatures from the two techniques are equivalent within their respective uncertainties. There is a slight indication that spectroscopic temperatures may be systematically higher, with 66 % of the stars lying above the line, however the effects on the abundance analysis are negligible and do not change any conclusions.

2.10.2. *Surface Gravity: Spectroscopic Versus Physical*

The surface gravity was determined from Hipparcos data (i.e. physical surface gravities) and spectroscopically via ionization balance. In Figure 2, the spectroscopic surface gravity is plotted versus the physical surface gravity. The line shows the trend for the gravities being equal. Within their respective uncertainties, the surface gravities are equal.

3. RESULTS AND DISCUSSION

The primary goal of the paper is to determine if the kinematically defined Wolf 630 Moving Group represents a stellar population of a single age and chemical composition. The sample stars have been plotted in the HR diagram (Figure 7) to determine if they are coincident with a single evolutionary sequence. The sequence traced by the majority of stars coincides with a Yale-Yonsei isochrone (Demarque et al. 2004) of 2.7 ± 0.5 Gyr with

an assumed solar metallicity. In attempting to qualitatively use ages as a constraint for establishing membership in a distinct evolutionary sequence, it will be assumed that the isochrone which fits the majority of the sample provides a reasonable estimate of the age range of a dominant coeval group, if it indeed exists.

The abundance results are presented in Table 5 and as plots of $[X/H]$ versus temperature (Appendix). Lithium and oxygen abundances were also derived, but they are presented and discussed separately as the approach utilized for these abundance results involved synthesis (Li) or use of the MOOG *blends* driver (O). In order to visually present the abundance results, the metallicity distribution of the entire sample is presented in the form of a “smoothed histogram” in Figure 3. This distribution has been generated by characterizing each star with a gaussian centered on its mean $[Fe/H]$ with standard deviation equal to the $[Fe/H]$ uncertainty. The distributions are summed to yield a final smoothed histogram and have been renormalized to a unit area. In this manner, the distributions include uncertainties in abundances, making them useful for a visual examination of the complete sample to discern if any stars yield abundances that deviate from the sample as a whole. The distribution is clearly not unimodal or symmetric. It is dominated by a near-solar metallicity peak and two smaller peaks at $[Fe/H] \sim -0.50$ and $[Fe/H] \sim +0.30$. It is clear that our Wolf 630 moving group sample is not characterized by a single chemical composition.

3.1. Approach to Chemically Tagging

While our entire sample cannot be characterized by a single chemical abundance, we can investigate whether there is a dominant subsample having common abundances and age. This is done by eliminating stars that are clearly outliers, using arguments based on extreme abundances, evolutionary state (inferred from HR diagram positions, lithium abundance, chromospheric activities and surface gravities) or a combination thereof. These members will be classified as “unlikely” members of a dominant homogeneous group. In this way we can, for example, establish a subsample that is characterized by a dominant $[Fe/H]$, if it exists. Stars with such an $[Fe/H]$ will be classified as either “possible” or “likely” members of a chemically homogeneous, isochronal population having common kinematics. The final distinctions between “possible” and “likely” will be made based on evolutionary status and additional abundance information inferred from lithium, alpha elements and iron peak elements. Particular interest is paid to the iron abundance, $[Fe/H]$, as it is considered the most well determined abundance, primarily due to the quality and size of the Fe line sample.

The quantitative constraint adopted for determining chemical homogeneity was to re-

quire that a star’s abundance, within its uncertainty, rest within a metallicity band centered on the weighted mean abundance of stars in the sample. The half-width of this band was conservatively taken to be 3 times the uncertainty in the weighted mean. This approach was followed in an iterative fashion where whenever a star was determined to be an “unlikely” member of a dominant chemical group it was removed from the sample and a new weighted mean and band size was found. In this manner, a common abundance for the sample was converged to for each element (except Lithium and Oxygen). Examples of the band plots for $[\text{Fe}/\text{H}]$ versus T_{eff} is given in Figure 4, where $[\text{Fe}/\text{H}]$ is plotted versus temperature. The solid line gives the weighted mean $[\text{Fe}/\text{H}]$ while the dotted lines give the $3\text{-}\sigma$ uncertainties in this mean, i.e. the abundance band.

This visual analysis from examining the abundance distributions served as a guide for identifying the clearly unlikely members. Abundance information alone was used to constrain giant star membership in a dominant chemical group, as robust discriminants of age are unavailable. Many of the dwarfs lay above the main sequence, leading to the question of if they might be pre-or-post main sequence objects. Consequently a diagnostic was needed to constrain evolutionary status for these dwarf and subgiant stars. The full analysis, therefore, examined each star individually, utilizing abundances and information on evolutionary status (inferred from chromospheric activities, isochrone ages and surface gravities) to classify each star in its appropriate category (unlikely, possible or likely).

Figure 6 shows the absolute lithium abundance versus effective temperature for the little-evolved stars in our sample and for a sample of dwarf stars in the Pleiades, Hyades, NGC752 and M67. The lithium abundances of the sample stars are plotted with each cluster: filled hexagons are dwarfs, filled triangles are upper limits for dwarfs, open hexagons are subgiants (as inferred from HR-diagram positions and apparently low levels of chromospheric activity) and open triangles are upper limits for subgiants. Accepted ages are given for each of the respective clusters, with the Pleiades trend being used as a baseline to indicate that a star is likely to be young (i.e. if a star has a lithium abundance which rests in the Pleiades lithium abundance trend it is likely a young star).

3.2. Final Membership

With the considerations above, the 34 stars in the sample have been classified as unlikely, possible and likely members of a common chemical, temporal and kinematic assemblage. There were a total of 13 stars removed from group membership due to classification as unlikely members. If the remaining 21 stars classified as possible and likely are considered to represent a chemically distinct group, then out of the original kinematically defined sample,

$\sim 60\%$ remain members of a kinematically and chemically related group with a common 2-3 Gyr age insofar as we can tell.

The final evolutionary sequence traced by the possible and likely members is presented in Figure 7, with possible members plotted in red and likely members plotted in green. The group is reasonably well traced by an evolutionary sequence of ~ 2.7 Gyr (solid line) with lower and upper limits of 2.2 Gyr and 3.2 Gyr (dashed lines). The dwarf members, HIP 41484, HIP 105341, HIP 14501 and HIP 43557, have positions that place them slightly above the main sequence; however, based on lithium abundances, none of the stars are believed to be pre-main sequence objects and surface gravities are all consistent with dwarf status. The giants HIP 3992, HIP 34440 and HIP 3455 appear to form a red giant clump. The remaining members all lay on the best fit isochrone within their respective uncertainties. Thus the possible and likely members we identify can be characterized by a distinct evolutionary sequence of 2.7 ± 0.5 Gyrs.

The final UV kinematic phase space plot is presented in Figure 8, where possible members are again red and likely members are green. For our initial full sample, the RMS U and V velocities are 23.92 and 34.46 kms^{-1} , respectively. In the final subsample of group members, $U_{RMS}=25.21 \text{ kms}^{-1}$ and $V_{RMS}=35.8 \text{ kms}^{-1}$, therefore the kinematic identity has not been significantly altered by the requirement of chemical and temporal coherence to establish group membership, which points to the necessity to utilize criteria other than kinematics to robustly link members of moving groups.

The weighted mean abundances of the final possible and likely members of a dominant chemical group are presented in Table 10. The quoted errors are the uncertainties in the weighted mean. In order to explore the homogeneity of our samples a reduced chi-squared statistic is presented for each element assuming a constant mean abundance. Performing this test for $[\text{Fe}/\text{H}]$ for warm stars ($T \geq 5000 \text{ K}$) in the Hyades cluster sample data from Schuler et al. (2006), yields a χ^2_ν of 1.303. For a set of 7 Pleiades stars from Schuler et al. (2003), the reduced chi-squared in $[\text{Fe}/\text{H}]$ is 1.818. Note that the cool stars were removed from the calculation as they are believed to be impacted by overexcitation/ionization effects. From these chi-squared values, we estimate the Hyades and Pleiades are chemically homogeneous with a roughly 2-sigma significance. With these open clusters assumed to be chemically homogeneous, an approximate reduced chi-squared of ≤ 2 , therefore, provides a rough quantitative indication of homogeneity. The χ^2_ν is presented for the full sample of 34 stars ($\chi^2_{\nu all}$), the final sample of 21 possible and likely group members ($\chi^2_{\nu group}$) and the 11 likely members ($\chi^2_{\nu likely}$). First, the very large $\chi^2_{\nu u}$ for the full sample confirms that the initial kinematically defined sample of alleged Wolf 630 members is clearly not chemically monolithic. The decrease in reduced chi-squared between the full sample and the chemically

distinct subsample demonstrates that chemically discrepant stars have been removed. Even in the likely subsample the χ^2_ν values remain uncomfortably large for Na and Al. Discussion of these discrepancies is reserved for a later section.

Considering the reduced chi-squared for other homogeneous open cluster samples is comparable to the reduced chi-squared for the possible and likely members of the sample across multiple elements, the chosen sample is considered to represent a chemically consistent group with a weighted average metallicity of $[\text{Fe}/\text{H}] = -0.01 \pm 0.02$ (uncertainty in the weighted mean). Using precise chemical tagging of the 34 star sample of the Wolf moving group, a single evolutionary sequence of 2.7 ± 0.5 Gyr and $[\text{Fe}/\text{H}] = -0.01 \pm 0.02$ has been identified for a subsample of 19 stars.

3.3. Open Clusters and Moving Groups: Chemically Tagging the Disk

We present additional results here that illustrate the application of moving group field star members in exploring stellar and chemical evolution in the Galactic disk.

3.3.1. Na and Al Abundances

The abundances of Na and Al appear to be enhanced for some of the stars in the sample. Similar enhancements have been observed in many open clusters. Most recently, an analysis of abundances in the Hyades cluster found abundance enhancements in Na and Al of 0.2-0.5 dex in giant stars when compared with dwarfs (Schuler et al. (2009)) in line with observations of giant stars in old open clusters (Friel et al. (2005), Jacobson et al. (2008)). These enhancements can be compared to those observed in the group members of this work.

Plots of $[\text{Na}/\text{Fe}]$ (top panel) and $[\text{Al}/\text{Fe}]$ (bottom panel) versus surface gravity are presented in Figure 9. For the members of the group, the Na and Al enhancements are relatively modest, as seen in a relatively slight upward shift in abundances between dwarfs and subgiants. The giant abundances, in general, can be brought into agreement with dwarf abundances with downward revisions of 0.1-0.2 dex, consistent with NLTE corrections found in field clump giants with surface gravities down to $\log g = 2.10$ (Mishenina et al. (2006)). The single star which has greatly enhanced $[\text{Na}/\text{Fe}]$ and $[\text{Al}/\text{Fe}]$, HIP 114155, is an evolved, metal poor red giant with enrichments of 0.53 dex and 0.51 dex, comparable to those found by Schuler et al. (2009). According to the NLTE correction table of Takeda et al. (2003), the recommended NLTE correction is at most -0.10, although the calculations performed do not extend below a temperature of 4500 K. Gratton et al. (1999) performed an extensive

set of NLTE corrections for Na, and based on their results, there is a recommended NLTE correction of ~ 0.20 dex. Even considering these corrections, the Na abundance remains enhanced. Although there are few NLTE corrections for Al in the literature, Andrievsky et al. (2008) suggest NLTE corrections of roughly 0.60 dex upward. This is opposite to the necessary correction to remove the enhancement, however the corrections are for low-metallicities ($[\text{Fe}/\text{H}] \approx -2.00$). Further NLTE calculations for cool, moderately low metallicity giant like HIP114155 are needed to determine whether the enhanced abundances in this star are a result of NLTE effects.

The other points of interest in Figure 9 are the two dwarfs with the greatest surface gravities ($[\text{Na}/\text{Fe}] = -0.38$ in HIP105341 and $[\text{Na}/\text{Fe}] = -0.33$ in HIP5027). Closer inspection shows that these are the two coolest dwarfs in the sample, perhaps pointing to overexcitation/ionization as a culprit for decreased abundances, similar to overexcitation/ionization effects observed in cool open cluster dwarfs (Schuler et al. (2003), Yong et al. (2004), King & Schuler (2005) and Schuler et al. (2006)).

Similar effects are not apparent for $[\text{Al}/\text{Fe}]$. A single Na line was measurable with a relatively low excitation potential of 2.10 eV, while two Al lines of 3.14 eV and 4.02 eV were used. Additionally, the ionization potential of Al is ~ 0.9 eV higher than for Na. These differences are qualitatively consistent with those needed for overexcitation/overionization to be manifest. This can be further explored by comparing abundances from Fe I and Fe II.

3.3.2. *Overexcitation and Overionization in Cool Dwarfs: Fe I and Fe II Abundances*

In order to more closely examine the possible effects of overexcitation and overionization for the sample, abundances have been derived from Fe I and Fe II lines using physical surface gravities (spectroscopic gravities are unsuitable for this purpose since ionization balance forces agreement between abundances of Fe I and Fe II). Refer to Figure 10 where the difference in abundances between ionized and neutral Fe are plotted versus temperature. For stars warmer than 4500 K the general trend reveals no overionization within the uncertainties. The same two coolest dwarfs which evince unusually low $[\text{Na}/\text{Fe}]$, show large degrees of Fe overionization,

Source of overionization in cool dwarfs are not well-understood, however, one possible explanation is that the stars are active young dwarfs and, thus, heavily spotted. Recent work suggests that heavily spotted stars have radii which are “puffed” compared to standard stellar models (Torres & Ribas (2002), Morales et al. (2008)). An increased radius would decrease the surface gravity of the star compared to unspotted analogs, which would result in increased

Fe II line strengths via overionization. In order to explore the viability of this explanation, the radius that corresponds to the surface gravity needed to eliminate the abundance difference between $[\text{Fe II}/\text{H}]$ and $[\text{Fe I}/\text{H}]$ was determined for HIP5027. A surface gravity of 3.57 was found to produce agreement between abundances from Fe I and Fe II, holding temperature and microturbulence constant. From Yale-Yonsei isochrones, a mass of $0.66 M_{\odot}$ is assumed. The radius for this gravity is $R=2.19 R_{\odot}$. The radius corresponding to this mass and the physical surface gravity of $\log g=4.70$ is $R=0.60 R_{\odot}$. From Morales et al. (2008) an upper limit that can be expected for radius changes in this “spotted” regime is $\sim 10\%$, well beneath the radius change implied by the necessary surface gravity change to eliminate overionization and well outside of the uncertainty in the physical surface gravity. This points to a more likely scenario of significant NLTE effects yielding increased overionization as a function of decreasing temperature as observed in many cool open cluster dwarfs (Yong et al. (2004), Schuler et al. (2006)).

3.3.3. *Oxygen Abundances: Moving Groups Versus Open Clusters*

Abundances for the $\lambda 7771$, $\lambda 7774$, $\lambda 7775$ high excitation potential oxygen triplet have been derived from equivalent widths. Since abundances derived from the triplet are believed to be enhanced by NLTE effects, corrections from the work of Takeda (2003) have been applied to derive NLTE corrected abundances from the triplet lines. The equivalent widths for the triplet, the LTE oxygen abundances, and the final NLTE oxygen abundances are shown in Table 7.

The $\lambda 7774 \text{ \AA}$ and $\lambda 7775 \text{ \AA}$ lines appear to be enhanced as a general function of decreasing temperature in both dwarfs (Figure 11) and giants. A similar enhancement of the central line (7774.1 \AA) in Hyades giants was noted by Schuler et al. (2006). They believed this enhancement to be due to a possible blend with an Fe I feature at 7774.00 \AA . While the nature of any blending for the reddest feature (7775 \AA) is unclear, visual inspection of the spectral line reveals a slight asymmetry, possibly indicating a blend. The distinct increase in $[\text{O}/\text{H}]$ abundances derived from the red features of the triplet as a function of decreasing temperature suggest that only the blue line (7771.1 \AA) of the triplet should be used for oxygen abundance determinations in cooler stars.

In order to test the possibility of an Fe blend as discussed above, two cool stars of the sample with no measurable oxygen abundances (HIP5027 and HIP105341) were examined to see if they showed any indications of an Fe blending feature near 7774 \AA . In HIP5027 a possible detection of a feature at 7774 \AA was found to have a measured equivalent width of roughly 6.0 m\AA . This strength is not inconsistent with the expected contribution required

from two nearby Fe I features at 7773.979 Å and 7774.06 Å for the derived Fe abundance.

Neglecting the two red triplet lines in the cool dwarfs, the [O/H] trend of the our dwarf sample is plotted along with the Pleiades trend from Schuler et al. (2004) (where [Fe/H]=0.00 was assumed to calculate [O/Fe]), and the Hyades trend of Schuler et al. (2006) (where [Fe/H]=+0.13 was assumed to calculate [O/Fe]) in Figure 12. Using $\lambda 7772$ triplet-based [O/H] abundances in 45 Hyades dwarfs, they found a remarkable increase in [O/H] as a function of decreasing temperature for stars with $T_{eff} \leq 5400$ K. The increase of [O/H] in the ~ 120 Myr old Pleiades appeared to be steeper than that in the ~ 625 Myr old Hyades, perhaps pointing to an age-related effect whereby [O/H] enhancements in cooler stars decrease as a function of increasing age.

Our field dwarfs do not show a drastic increase in abundance as a function of decreasing temperature. The single star that appears to reside within the increasing Hyades trend at cooler temperatures is metal weak (HIP 42499, [Fe/H]=-0.56), resulting in [O/Fe]=+0.47. The enhanced [O/Fe] ratio at this low metallicity is unsurprising and coincides with the characteristic field dwarf enhancements observed as a function of decreasing temperature for oxygen in other metal poor field stars (Abia & Rebolo 1989). If the abundance trend observed by Schuler et al. (2004) and Schuler et al. (2006) is age dependent, the lack of a distinct trend of increasing [O/Fe] with decreasing abundance may point to the stars in the sample being older than the Hyades, not inconsistent with the 2.7 Gyr age of the dominant subsample identified above. If not an age-related effect, then an as yet unknown dichotomy between oxygen abundances in field stars and cluster stars would have to be explored with abundances of field stars of quantifiable age.

For the giant stars in the sample, oxygen abundances have been derived from the infrared triplet and from the forbidden line at $\lambda 6300.301$ Å, through use of the *blends* driver of MOOG, following the approach of Schuler et al. (2006).

In examining the giant triplet abundances, a similar effect as in the dwarfs is observed as temperatures decrease with enhancements in oxygen abundances derived from both the 7774 Å and 7775 Å lines. NLTE corrections were applied to the $\lambda 7771$ triplet abundances by interpolating within the grids of Takeda (2003). The results of these corrections are presented in Figure 13 where forbidden minus permitted [O/H] differences versus temperature are plotted. Notice that as the temperature decreases, the abundance from the redder lines of the triplet appear to be enhanced relative to the forbidden line. While the NLTE corrections decreased the abundance enhancements in the cooler stars of the sample, they did not eliminate them. This yields further evidence of blending effects in the reddest lines of the triplet as a function of cooler temperature. For the purposes of this paper, the oxygen abundances derived from the red features of the triplet will not be used.

In Figure 14 the difference in abundance from the forbidden oxygen line (6300.34 Å) and the NLTE corrected blue triplet line (7771 Å) is plotted versus temperature (top plot) and surface gravity (bottom plot). The dotted line shows a zero difference between the two abundances. The NLTE-corrected permitted oxygen abundances (7771 Å) appear to agree well with the forbidden oxygen abundance (6300 Å) indicating that the blue line of the triplet can provide a reliable oxygen abundance when proper care is taken to make the necessary NLTE corrections.

The single outlier is the highly evolved giant HIP 114155. The larger abundance from the blue triplet feature in this star is believed to be from NLTE effects that are not removed using the corrections of Takeda (2003) as the grid for the corrections does not extend below 4500 K. While the temperature extrapolation is sufficient for less evolved stars (i.e. NLTE triplet abundances in stars with surface gravities above 2.0 all agree with the forbidden abundance, even at temperatures below 4500 K), the corrections for more evolved stars, with surface gravities ~ 1.00 , are significantly larger. The good agreement between all other forbidden and blue triplet oxygen abundances indicates the inadequacy extrapolating the NLTE corrections in cool, evolved stars.

The final salient point to make regarding the oxygen abundances is to address the alleged CN blending feature previously discussed. As mentioned, Davis & Phillips (1963) list CN features at 6300.265 Å and two features at 6300.482 Å with gf values of 5.78E-3, 6.82E-3 and 2.01E-3. Recall that the inability to adequately calibrate a linelist including these features with a high resolution atlas of Arcturus led to the features not being utilized in the derivation of forbidden line oxygen abundances. With the good agreement between forbidden oxygen neglecting the CN features and the NLTE corrected blue line of the triplet in Figure 14, it is suggested that the CN blending features may not be important.

4. SUMMARY

The existence of spatially unassociated groups of stars moving through the solar neighborhood with common U and V kinematics has been explored for over half a century (Eggen 1958). Despite this long history, the exact origins of these so called moving groups is still a matter of some debate. The classical view contends that they are dissolved open clusters which have retained common kinematics and drifted into spatially elongated stellar streams. If this is indeed true, moving group members should possess similar characteristics to those of open cluster stars: particularly, common chemical abundances and residence along a distinct evolutionary sequence in an HR diagram.

In order to address the viability of moving groups being dissolved open clusters, we have performed a high resolution spectroscopic abundance analysis of a 34 star sample of the kinematically distinct Wolf 630 moving group, selected for its residence in a sparsely populated region of the UV plane in the solar neighborhood. Our abundance measurements reveal that the sample can not be characterized by a uniform abundance pattern. The individual stars have been closely scrutinized, making use of abundances, evolutionary state and qualitative age information to constrain membership as an unlikely, possible or likely member of a subsample with a dominant abundance trend and consistent age. There appears to be a group with a weighted mean of $[Fe/H]=-0.01 \pm 0.02$ (uncertainty in the weighted mean) that is composed of 19 stars. These final members are well traced by an evolutionary sequence of 2.7 ± 0.5 Gyr as determined from Yale-Yonsei isochrones (Demarque et al. 2004). Thus, the existence of moving groups as relic structures of dissolved clusters remains plausible based on the homogeneity of the subgroup identified above.

We have also explored some of the additional uses for abundances in moving groups in chemically tagging the galactic disk. We found evidence for overexcitation/overionization effects from both Na and from Fe I versus Fe II abundances in the coolest dwarfs of the sample, likely attributable to increasing NLTE effects as a function of cooling temperature. We find the necessity to apply NLTE corrections of 0.10-0.20 dex to Na abundances in giant stars. Finally, we derived oxygen abundances for the stars in the sample from both the forbidden line at 6300 Å and the near-IR triplet. First, we find evidence for blending in the IR triplet in both dwarfs and giant stars, possibly by Fe I features near the $\lambda 7774$ line. Second, we find that NLTE effects on O I in low $\log g$ cool giants are important and cannot be accounted for by extrapolating current NLTE calculations. Finally, we find reliable oxygen abundances from the forbidden line in giant stars and again find evidence of increased NLTE effects as a function of cooling temperature manifested in increased triplet derived abundances.

The authors would like to gratefully acknowledge support for this work provided by NSF grants AST-0908342 and AST-0239518. Furthermore, we would like to thank the referee for many useful comments which place the work into a broader context.

REFERENCES

- Abia, C., & Rebolo, R. 1989, ApJ, 347, 186
- Allende Prieto, C., Barklem, P. S., Lambert, D. L., &

- Andrievsky, S. M., Spite, M., Korotin, S. A., Spite, F., Bonifacio, P., Cayrel, R., Hill, V., & François, P. 2008, *A&A*, 481, 481
- Balachandran, S. 1990, *Cool Stars, Stellar Systems, and the Sun*, 9, 357
- Balachandran, S. 1995, *ApJ*, 446, 203
- Casagrande, L., Ramírez, I., Meléndez, J., Bessell, M., & Asplund, M. 2010, *A&A*, 512, A54
- Cutri, R. M., et al. 2003, *The IRSA 2MASS All-Sky Point Source Catalog*, NASA/IPAC Infrared Science Archive. <http://irsa.ipac.caltech.edu/applications/Gator/>,
- Davis, S. P., & Phillips, J. G. 1963, *Berkeley Analyses of Molecular Spectra*, Berkeley: University of California Press,
- Demarque, P., Woo, J.-H., Kim, Y.-C., & Yi, S. K. 2004, *ApJS*, 155, 667
- De Silva, G. M., Sneden, C., Paulson, D. B., Asplund, M., Bland-Hawthorn, J., Bessell, M. S., & Freeman, K. C. 2006, *AJ*, 131, 455
- De Silva, G. M., Freeman, K. C., Bland-Hawthorn, J., Asplund, M., & Bessell, M. S. 2007, *AJ*, 133, 694
- Eggen, O. J. 1958, *MNRAS*, 118, 65
- Eggen, O. J. 1965, *The Observatory*, 85, 191
- Eggen, O. J. 1969, *PASP*, 81, 553
- Eggen, O. J. 1970, *PASP*, 82, 99
- Fitzpatrick, M. J., & Sneden, C. 1987, *BAAS*, 19, 1129
- Friel, E. D., Jacobson, H. R., & Pilachowski, C. A. 2005, *AJ*, 129, 2725
- Girardi, L., Bressan, A., Bertelli, G., & Chiosi, C. 2000, *A&AS*, 141, 371
- Gratton, R. G., Carretta, E., Eriksson, K., & Gustafsson, B. 1999, *A&A*, 350, 955
- Gray, R. O., Corbally, C. J., Garrison, R. F., McFadden, M. T., Bubar, E. J., McGahee, C. E., O'Donoghue, A. A., & Knox, E. R. 2006, *AJ*, 132, 161
- Gray, D. F. 1981, *ApJ*, 245, 992
- Gray, D. F. 2005, *The Observation and Analysis of Stellar Photospheres*, 3rd Edition, by D.F. Gray. ISBN 0521851866. Cambridge, UK: Cambridge University Press, 2005

- Hinkle, K., Wallace, L., Valenti, J., & Harmer, D. 2000, Visible and Near Infrared Atlas of the Arcturus Spectrum 3727-9300 Å ed. Kenneth Hinkle, Lloyd Wallace, Jeff Valenti, and Dianne Harmer. (San Francisco: ASP) ISBN: 1-58381-037-4, 2000.,
- Holmberg, J., Nordström, B., & Andersen, J. 2007, *A&A*, 475, 519
- Jacobson, H. R., Friel, E. D., & Pilachowski, C. A. 2007, *AJ*, 134, 1216
- Jacobson, H. R., Friel, E. D., & Pilachowski, C. A. 2008, *AJ*, 135, 2341
- Johnson, D. R. H., & Soderblom, D. R. 1987, *AJ*, 93, 864
- Jones, B. F., Fischer, D., & Soderblom, D. R. 1999, *AJ*, 117, 330
- King, J. R., Deliyannis, C. P., Hiltgen, D. D., Stephens, A., Cunha, K., & Boesgaard, A. M. 1997, *AJ*, 113, 1871
- King, J. R., Stephens, A., Boesgaard, A. M., & Deliyannis, C. 1998, *AJ*, 115, 666
- King, J. R., Krishnamurthi, A., & Pinsonneault, M. H. 2000, *AJ*, 119, 859
- King, J. R., Villarreal, A. R., Soderblom, D. R., Gulliver, A. F., & Adelman, S. J. 2003, *AJ*, 125, 1980
- King, J. R., & Schuler, S. C. 2005, *PASP*, 117, 911
- Kupka, F., & Ryabchikova, T. A. 1999, *Publications de l’Observatoire Astronomique de Beograd*, 65, 223
- Kupka, F. G., Ryabchikova, T. A., Piskunov, N. E., Stempels, H. C., & Weiss, W. W. 2000, *Baltic Astronomy*, 9, 590
- Kurucz, R. L. 2005, *Memorie della Societa Astronomica Italiana Supplement*, 8, 189
- Mamajek, E. E., & Hillenbrand, L. A. 2008, *ApJ*, 687, 1264
- McDonald, A. R. E., & Hearnshaw, J. B. 1983, *MNRAS*, 204, 841
- Mishenina, T. V., Bienaymé, O., Gorbaneva, T. I., Charbonnel, C., Soubiran, C., Korotin, S. A., & Kovtyukh, V. V. 2006, *A&A*, 456, 1109
- Morales, J. C., Ribas, I., & Jordi, C. 2008, *A&A*, 478, 507
- Nordström, B., et al. 2004, *A&A*, 418, 989

- Perryman, M. A. C., & ESA 1997, The Hipparcos and Tycho catalogues. Astrometric and photometric star catalogues derived from the ESA *HIPPARCOS* Space Astrometry Mission, Publisher: Noordwijk, Netherlands: ESA Publications Division, 1997, Series: ESA SP Series vol no: 1200, ISBN: 9290923997 (set),
- Piskunov, N. E., Kupka, F., Ryabchikova, T. A., Weiss, W. W., & Jeffery, C. S. 1995, A&AS, 112, 525
- Ramírez, I., & Meléndez, J. 2005, ApJ, 626, 465
- Ryabchikova, T. A., Piskunov, N. E., Kupka, F., & Weiss, W. W. 1997, Baltic Astronomy, 6, 244
- Salasnich, B., Girardi, L., Weiss, A., & Chiosi, C. 2000, A&A, 361, 1023
- Schuler, S. C., King, J. R., Fischer, D. A., Soderblom, D. R., & Jones, B. F. 2003, AJ, 125, 2085
- Schuler, S. C., King, J. R., Hobbs, L. M., & Pinsonneault, M. H. 2004, ApJ, 602, L117
- Schuler, S. C., Hatzes, A. P., King, J. R., Kürster, M., & The, L.-S. 2006, AJ, 131, 1057
- Schuler, S. C., King, J. R., & The, L. -. 2009, arXiv:0906.4812
- Sestito, P., Randich, S., & Pallavicini, R. 2004, A&A, 426, 809
- Skuljan, J., Hearnshaw, J. B., & Cottrell, P. L. 1999, MNRAS, 308, 731
- Smith, V. V., et al. 2002, AJ, 124, 3241
- Snedden, C. A. 1973, Ph.D. Thesis,
- Soderblom, D. R., & Mayor, M. 1993, AJ, 105, 226
- Takeda, Y. 2003, A&A, 402, 343
- Takeda, Y., Zhao, G., Takada-Hidai, M., Chen, Y.-Q., Saito, Y.-J., & Zhang, H.-W. 2003, Chinese Journal of Astronomy and Astrophysics, 3, 316
- Taylor, B. J. 1994, Bulletin of the American Astronomical Society, 26, 1382
- Thevenin, F. 1990, A&AS, 82, 179
- Torres, G., & Ribas, I. 2002, ApJ, 567, 1140

- Tuominen, I. V., & Vilhu, O. 1979, *Liege International Astrophysical Colloquia*, 22, 355
- Valenti, J. A., & Fischer, D. A. 2005, *ApJS*, 159, 141
- van Leeuwen, F. 2007, *A&A*, 474, 653
- Yong, D., Lambert, D. L., Allende Prieto, C., & Paulson, D. B. 2004, *ApJ*, 603, 697

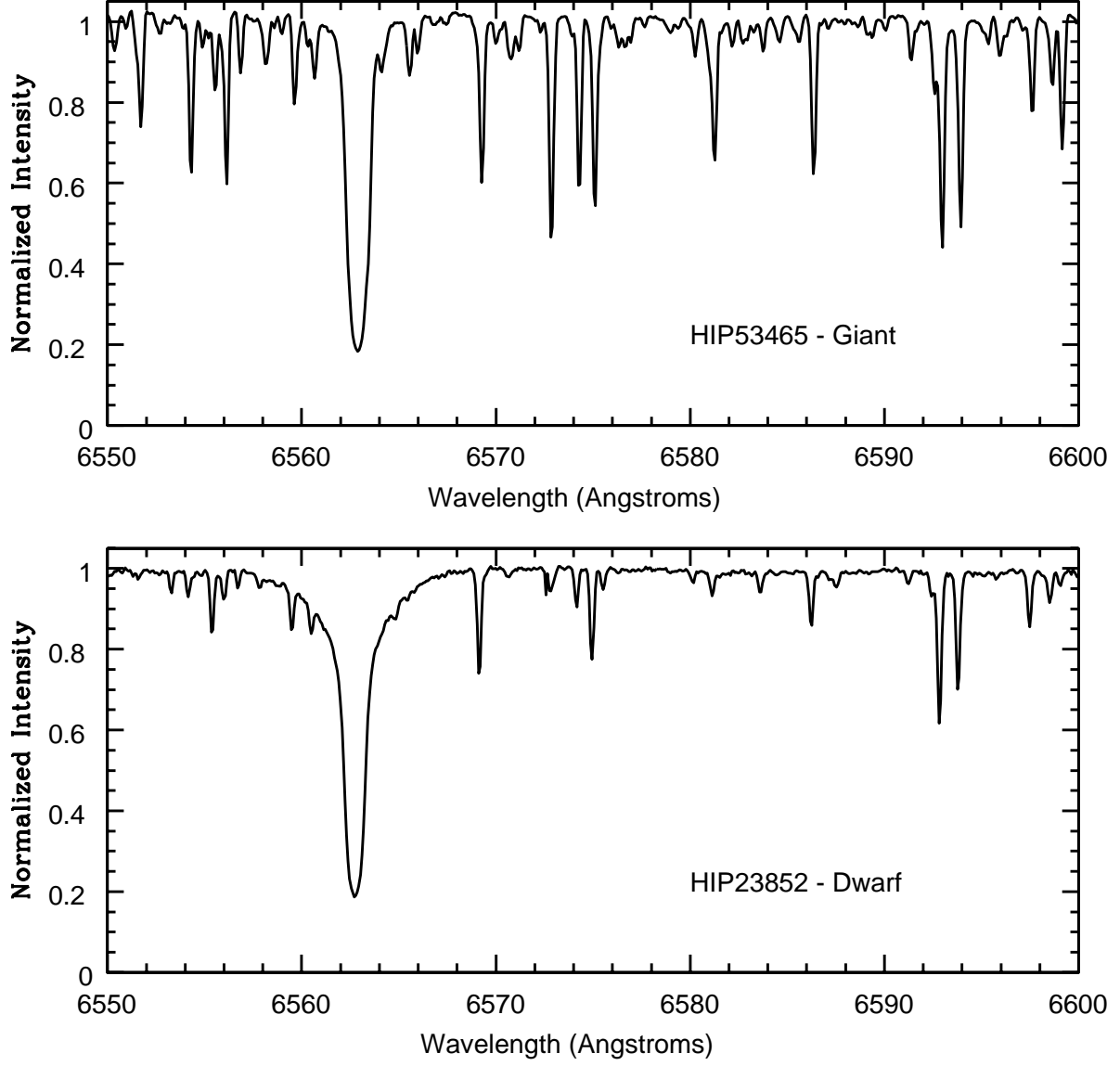


Fig. 1.— Sample normalized spectra of our 34 star sample. The top panel shows a giant star and the bottom displays a dwarf. The typical continuum level S/N in these spectra are ~ 200 .

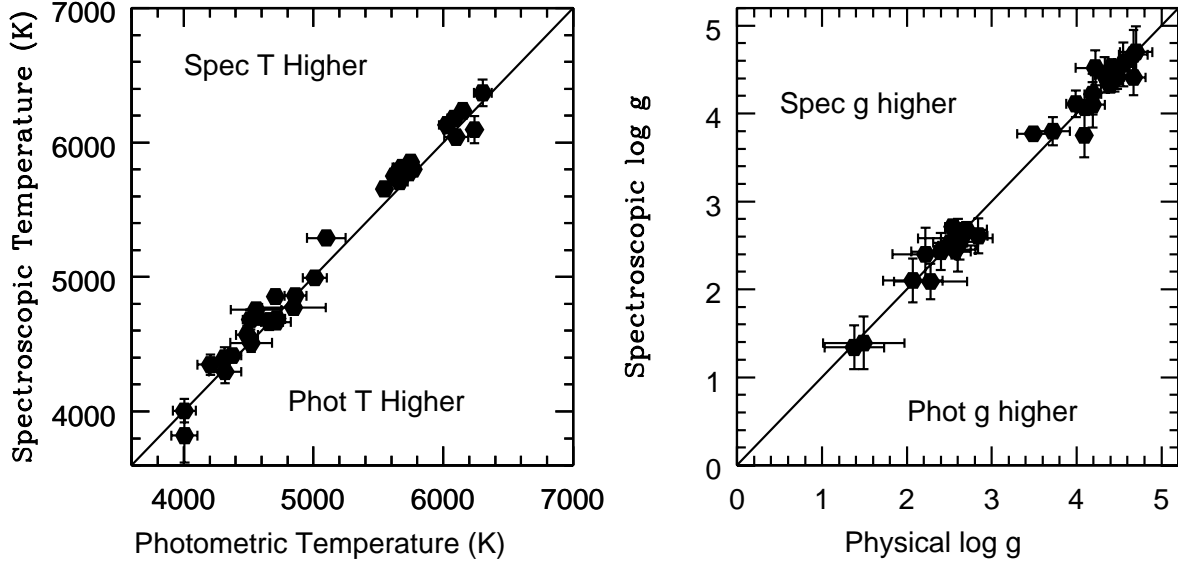


Fig. 2.— The spectroscopic temperatures are plotted versus photometric temperatures in the left plot and the spectroscopic gravities versus physical gravities are plotted in the right plot. The line is plotted to show perfect agreement between the two values. The differences between the spectroscopic and photometric parameters agree within the uncertainties in the respective mean differences.

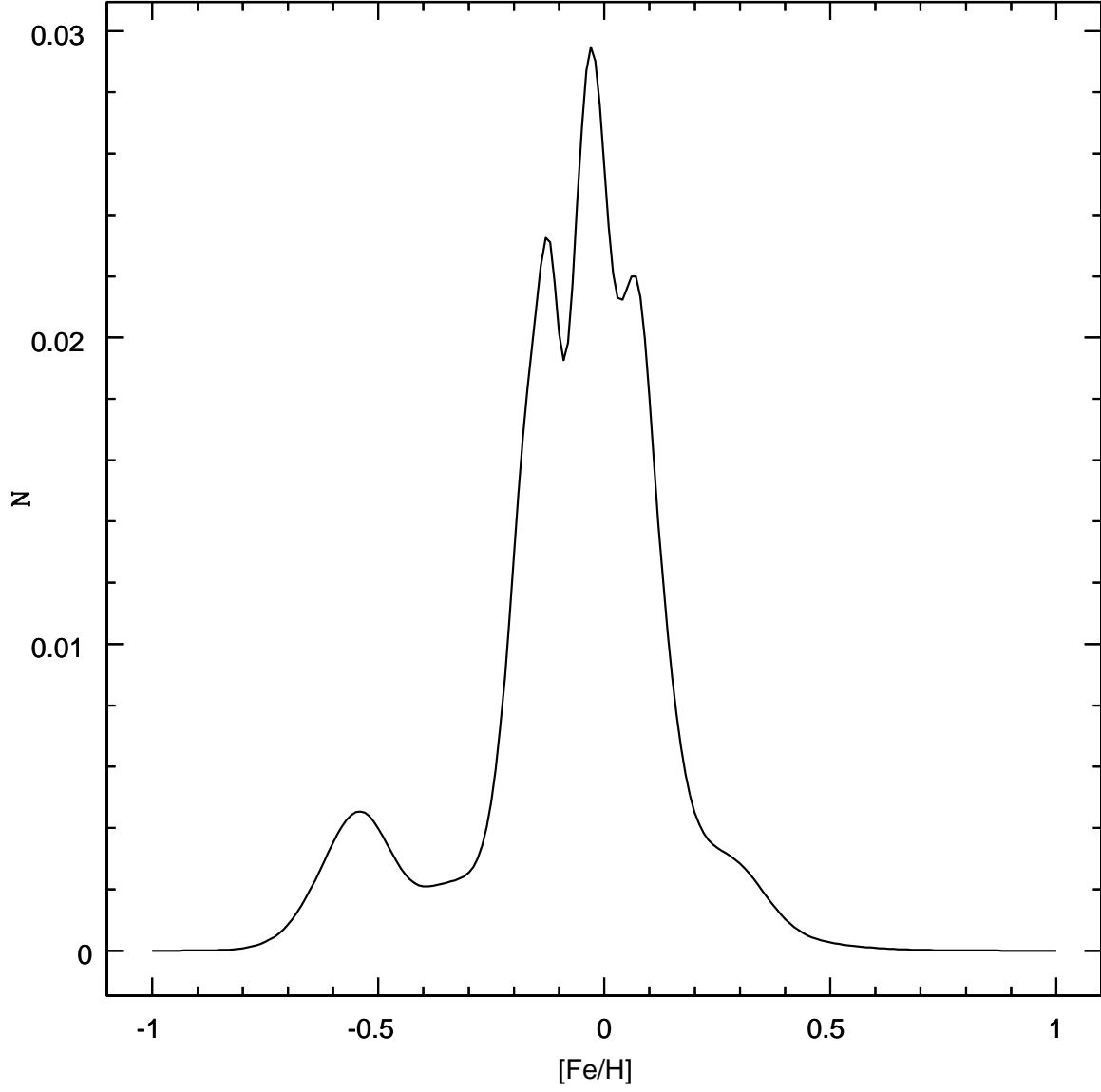


Fig. 3.— The metallicities of our 34 stars are plotted as guassians with central peaks at a given star’s metallicity and σ equal to the uncertainty in the $[\text{Fe}/\text{H}]$. The guassians are normalized to unit area and summed to yield the smoothed abundance histogram. The peak at $[\text{Fe}/\text{H}] \sim -0.50$ is from 3 low metallicity stars and the bump at $[\text{Fe}/\text{H}] \sim 0.30$ is from 2 high metallicity stars.

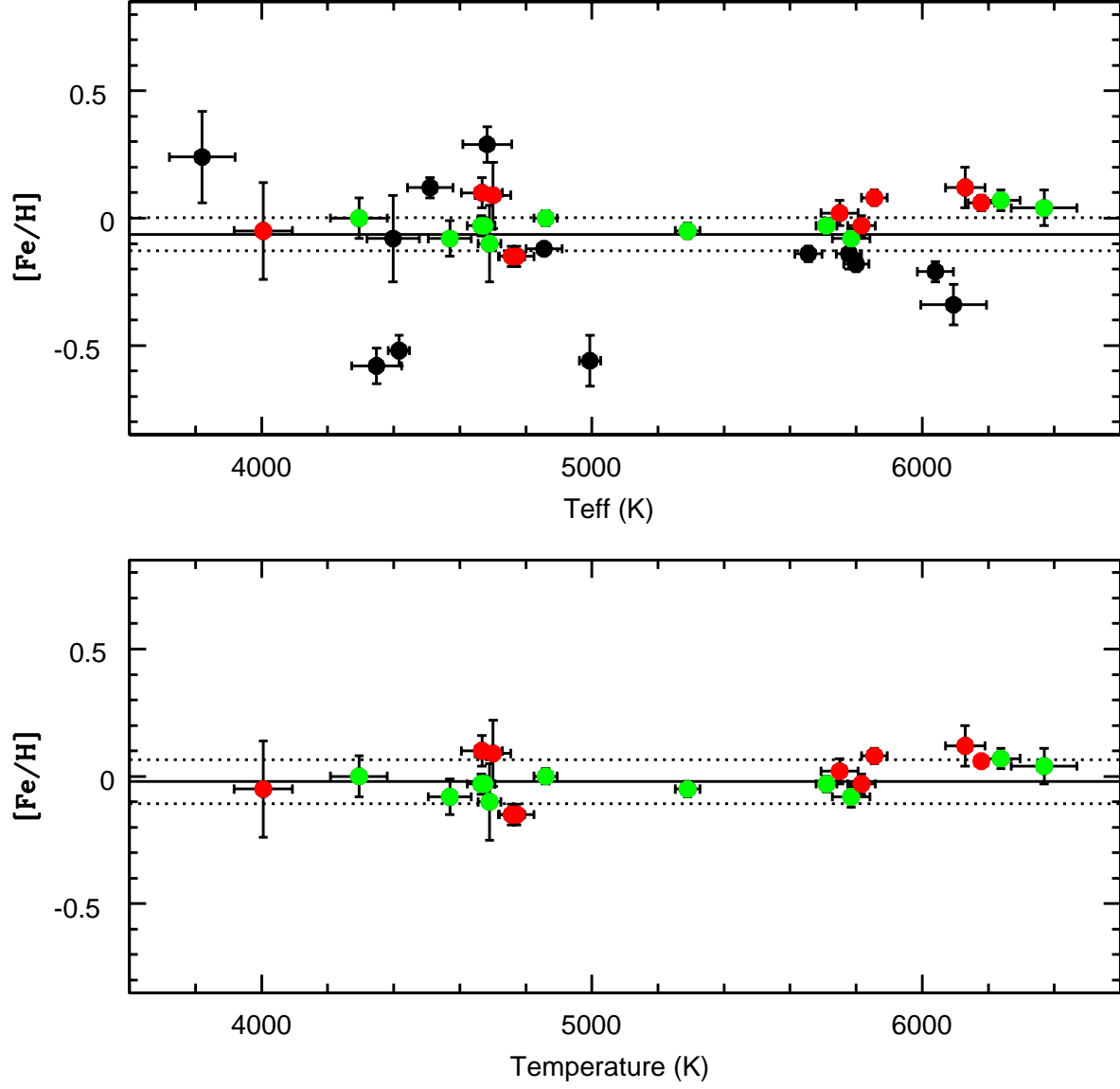


Fig. 4.— The $[\text{Fe}/\text{H}]$ is plotted versus temperature for the full sample of stars (top) and the possible (red) and likely (green) homogeneous members (bottom). The solid line gives the weighted mean of the sample while the dotted lines are 3σ deviations from this mean. If a star rests within the dotted lines (i.e. the abundance band) within its respective uncertainty, then it is considered homogeneous with the dominant sample. Those stars which rest far outside the abundance band in the full sample plot are iteratively removed as unlikely members until convergence to a dominant abundance is achieved, as seen in the bottom plot.

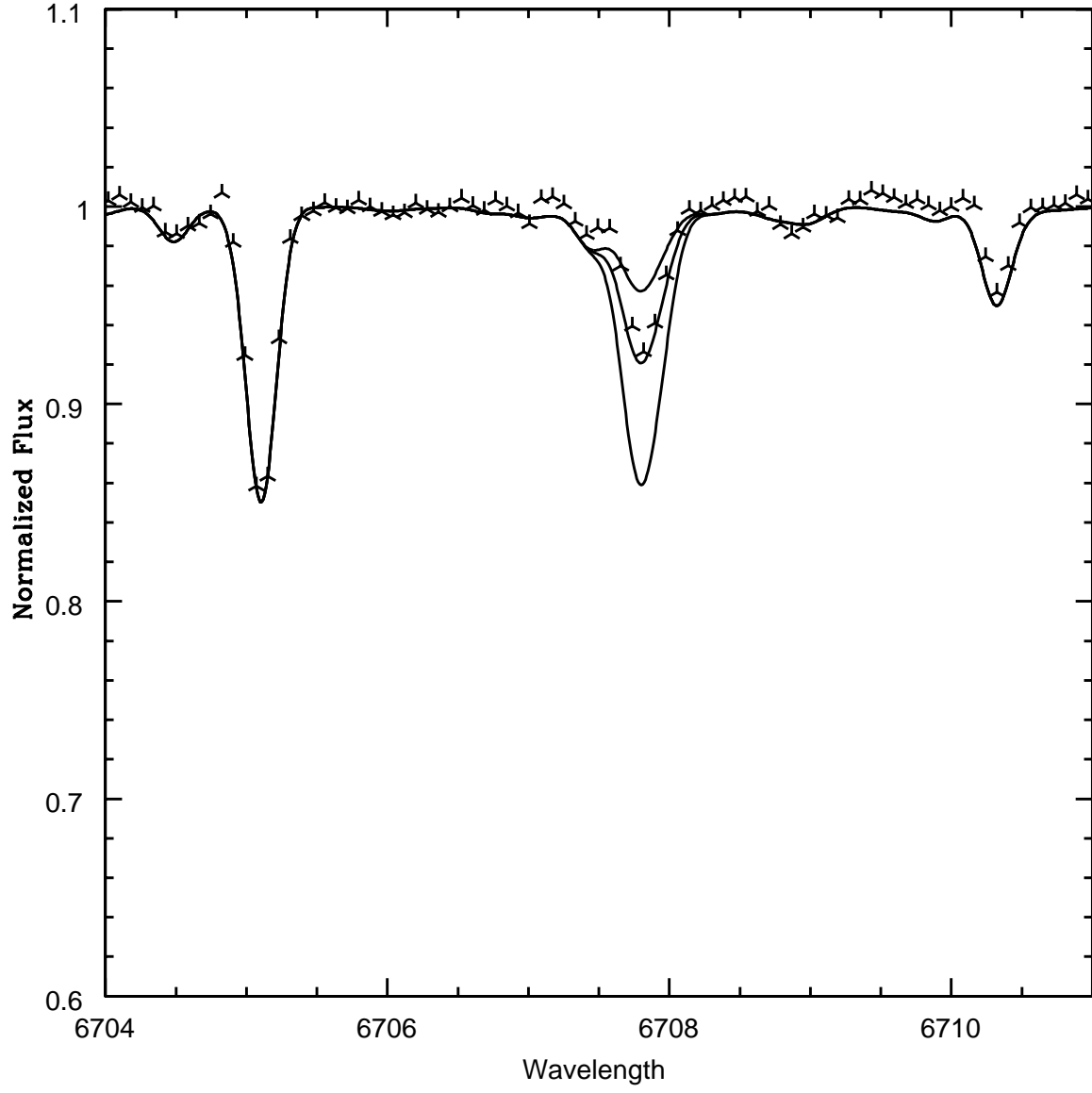


Fig. 5.— Sample lithium synthesis for HIP 23852. The crosses are the observed spectrum while the lines are lithium abundances of $\log N(\text{Li})=2.30$, 2.00 (best fit) and 1.97 .

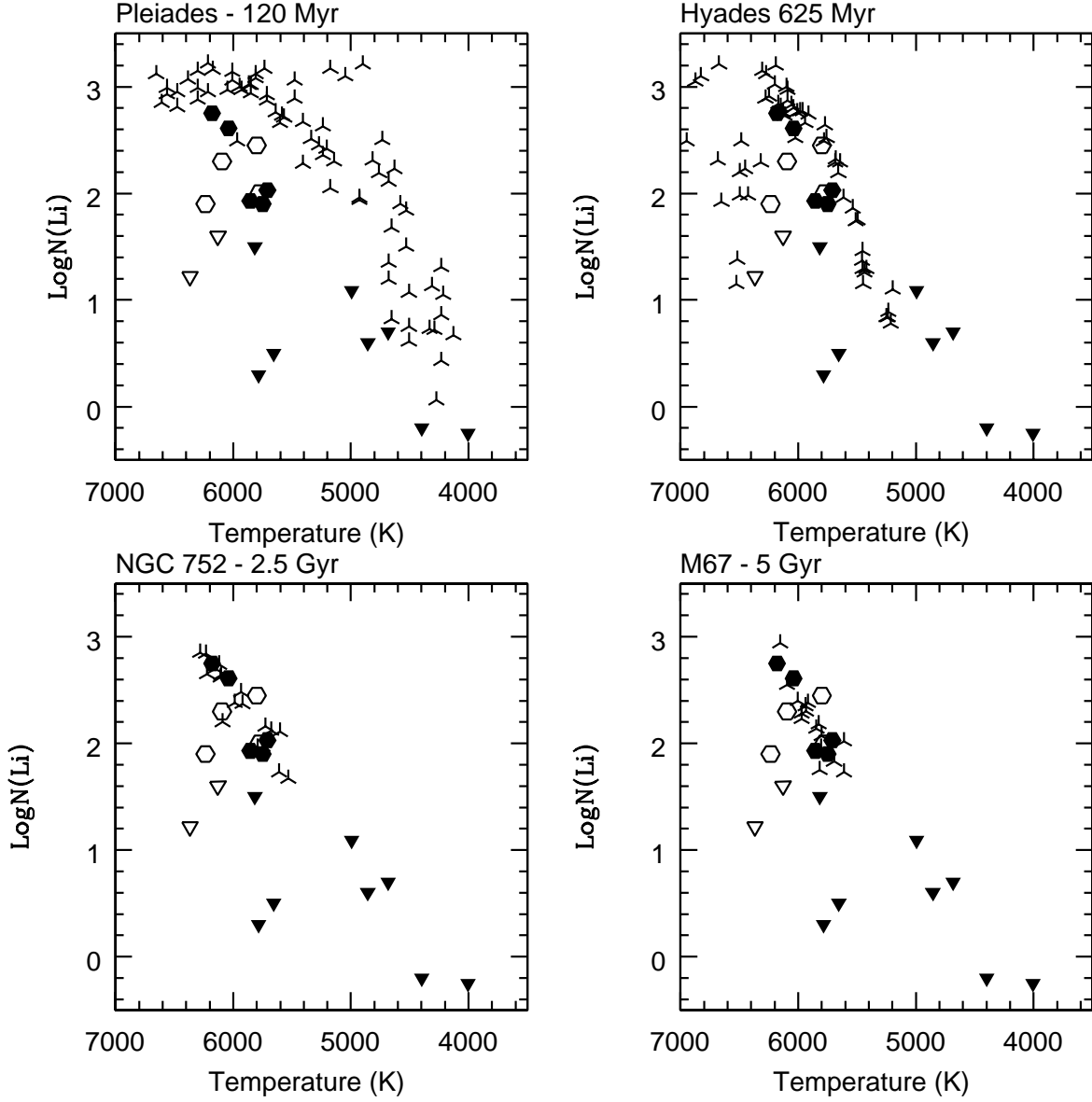


Fig. 6.— Lithium abundances for the Pleiades (top left-King et al. (2000)), the Hyades (top right-Balachandran (1995)), NGC752 (bottom left-Sestito et al. (2004)) and M67 (bottom right-Jones et al. (1999) (plotted as crosses) and our Wolf 630 candidates. Filled hexagons are for dwarfs, filled triangles are upper limits for dwarfs, open hexagons are for subgiants open triangles are upper limits for subgiants. Specific abundances for individual stars are discussed in more detail in the text.

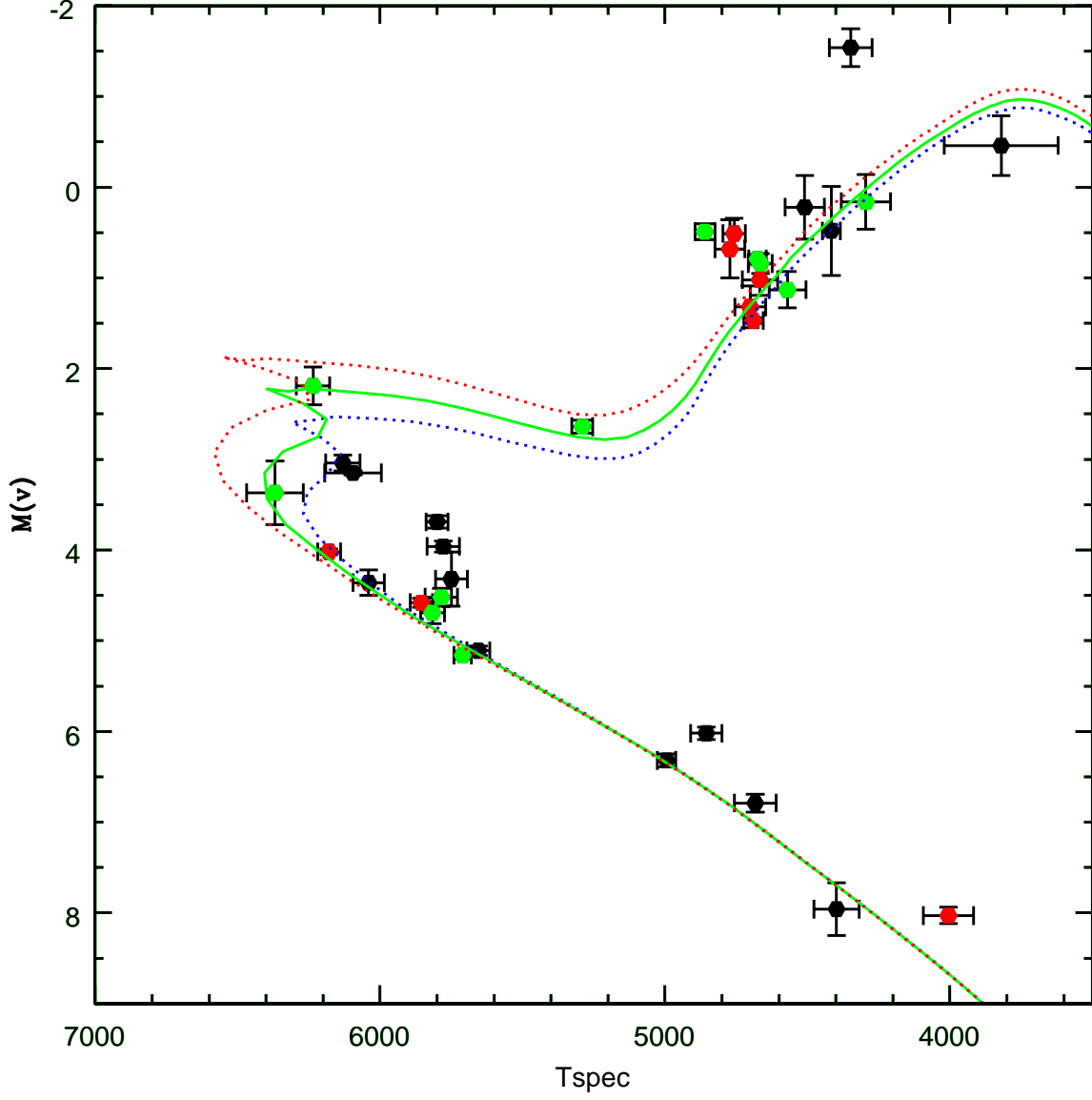


Fig. 7.— The HR diagram of the final candidate members of a common chemical group with the distinct UV kinematics of the classical Wolf 630 group. Green points are likely members while red points are possible members. Unlikely members are plotted as black points. Yale-Yonsei isochrones of 2.2, 2.7 and 3.2 Gyr are shown.

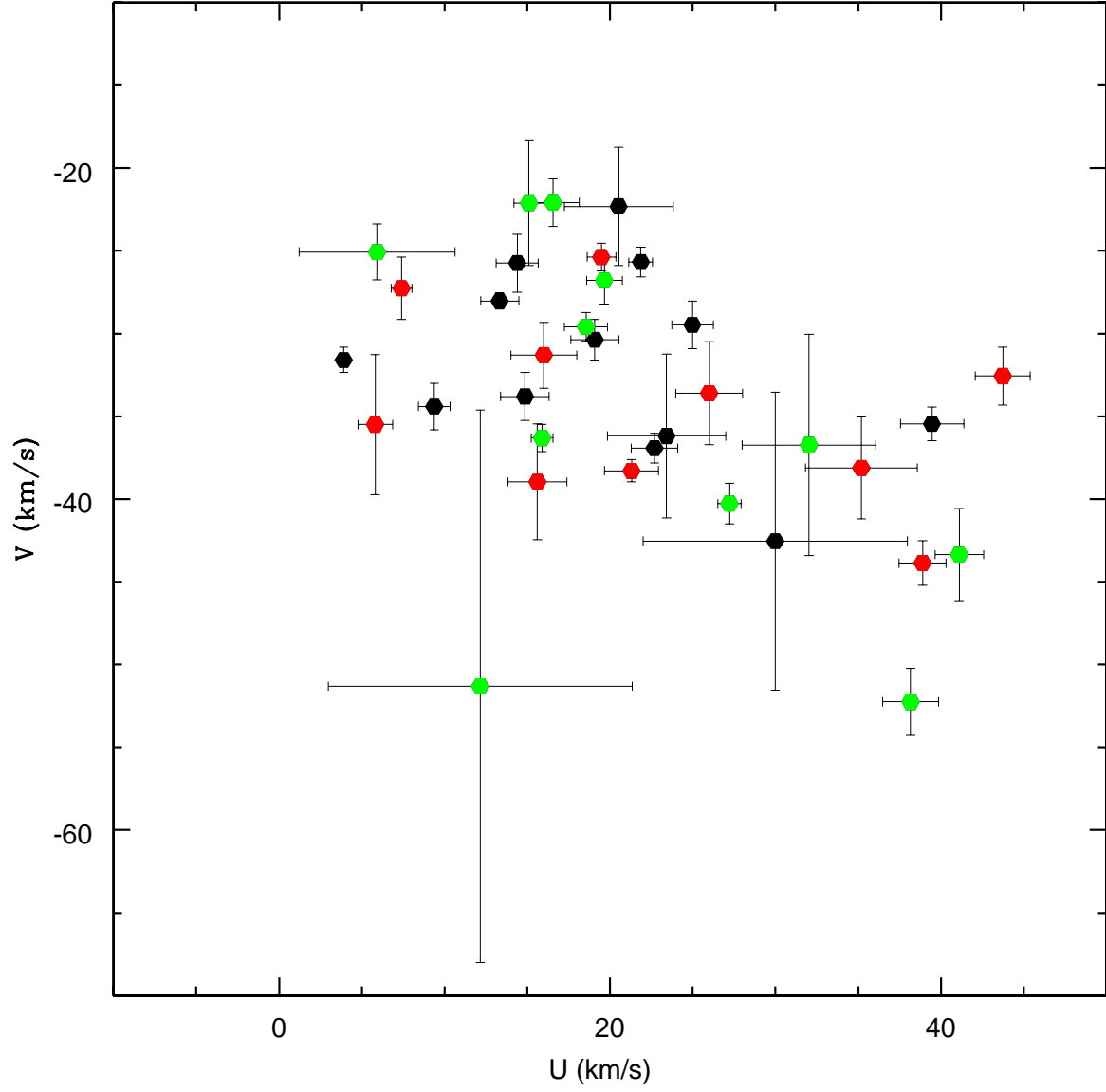


Fig. 8.— Plot of the U and V kinematics for the sample with likely members plotted in red and possible members in green. Black points are non-members

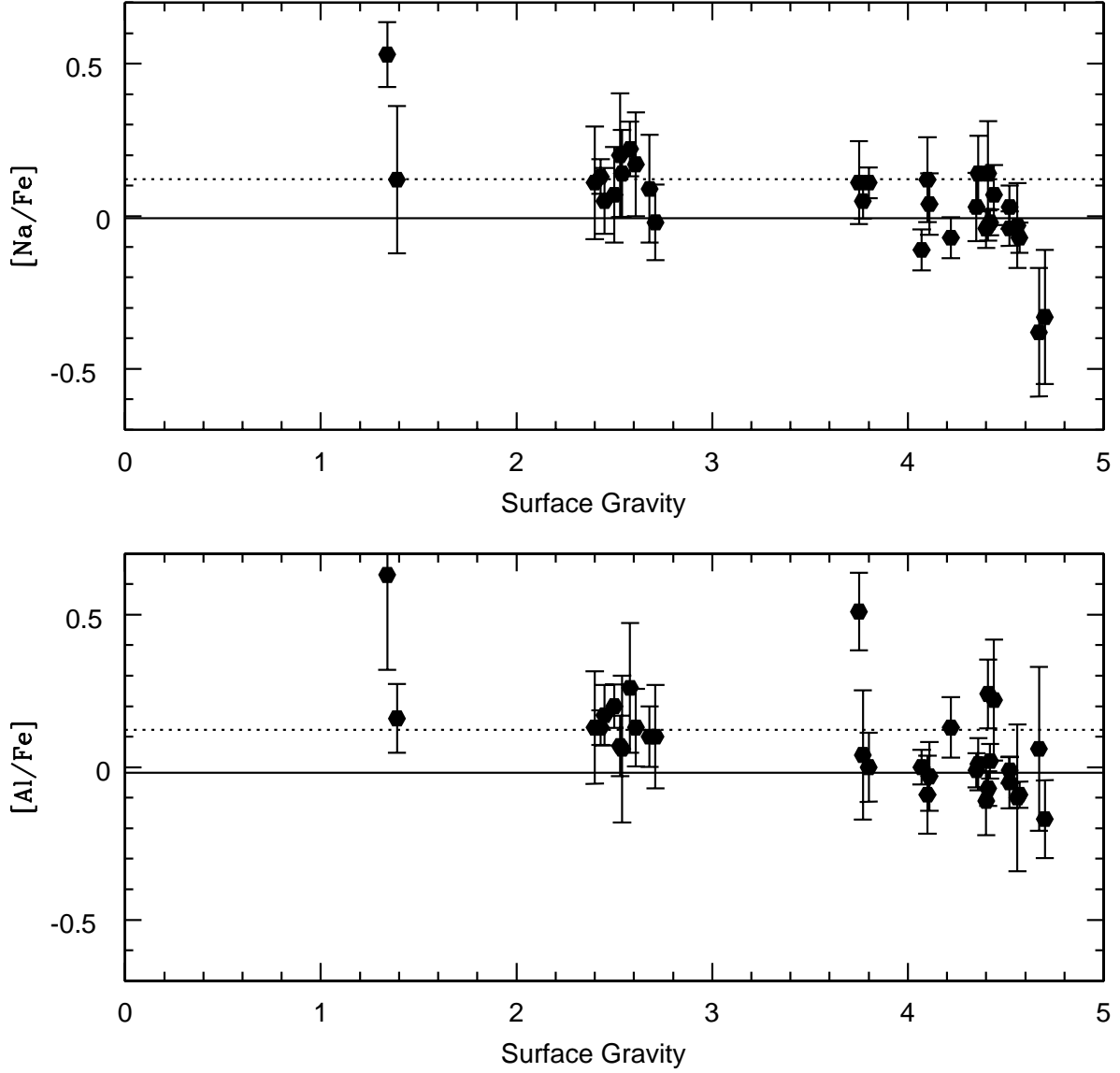


Fig. 9.— The abundances $[\text{Na}/\text{Fe}]$ (top) and $[\text{Al}/\text{Fe}]$ (bottom) for all stars with measurable lines of Na and/or Al are plotted versus surface gravity. The solid line gives the weighted mean $[\text{X}/\text{Fe}]$ for the dwarfs, neglecting the two with unusually low $[\text{Na}/\text{Fe}]$. The dotted line gives the weighted mean $[\text{X}/\text{Fe}]$ for the subgiants and giants, neglecting the giant with unusually high $[\text{Na}/\text{Fe}]$ and $[\text{Al}/\text{Fe}]$. Subgiant and giant abundances are ~ 0.10 dex higher than dwarfs.

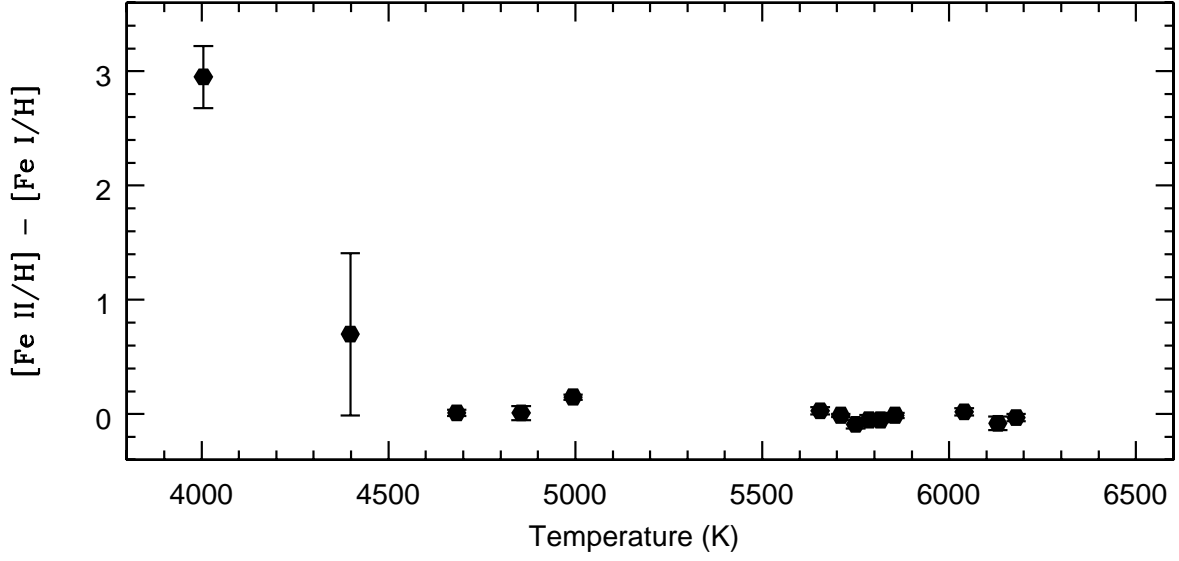


Fig. 10.— The difference $[\text{Fe II}/\text{H}] - [\text{Fe I}/\text{H}]$ is plotted versus temperature. Notice the clear overionization in the two coolest dwarfs of the sample.

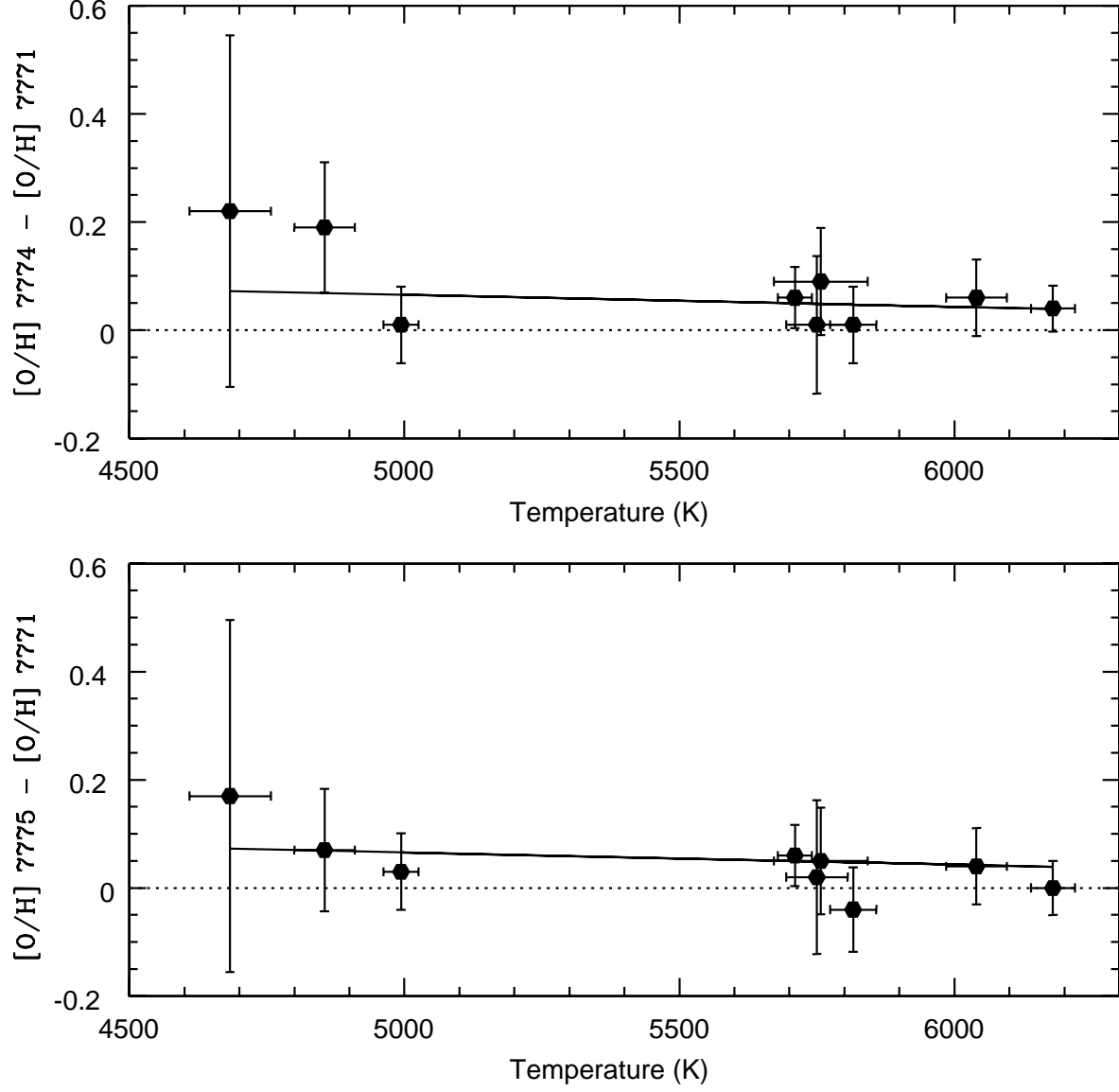


Fig. 11.— Differences in oxygen abundances for dwarf stars derived from the infrared triplet. The top plot shows the difference in the abundance from the 7774 line and the 7771 line. The difference in abundance between these two lines for the coolest two stars in the sample is of order 0.20 dex. The difference between the 7775 line and the 7771 line is slightly more modest, but the general trend is for the cooler stars to yield slight abundance enhancements.

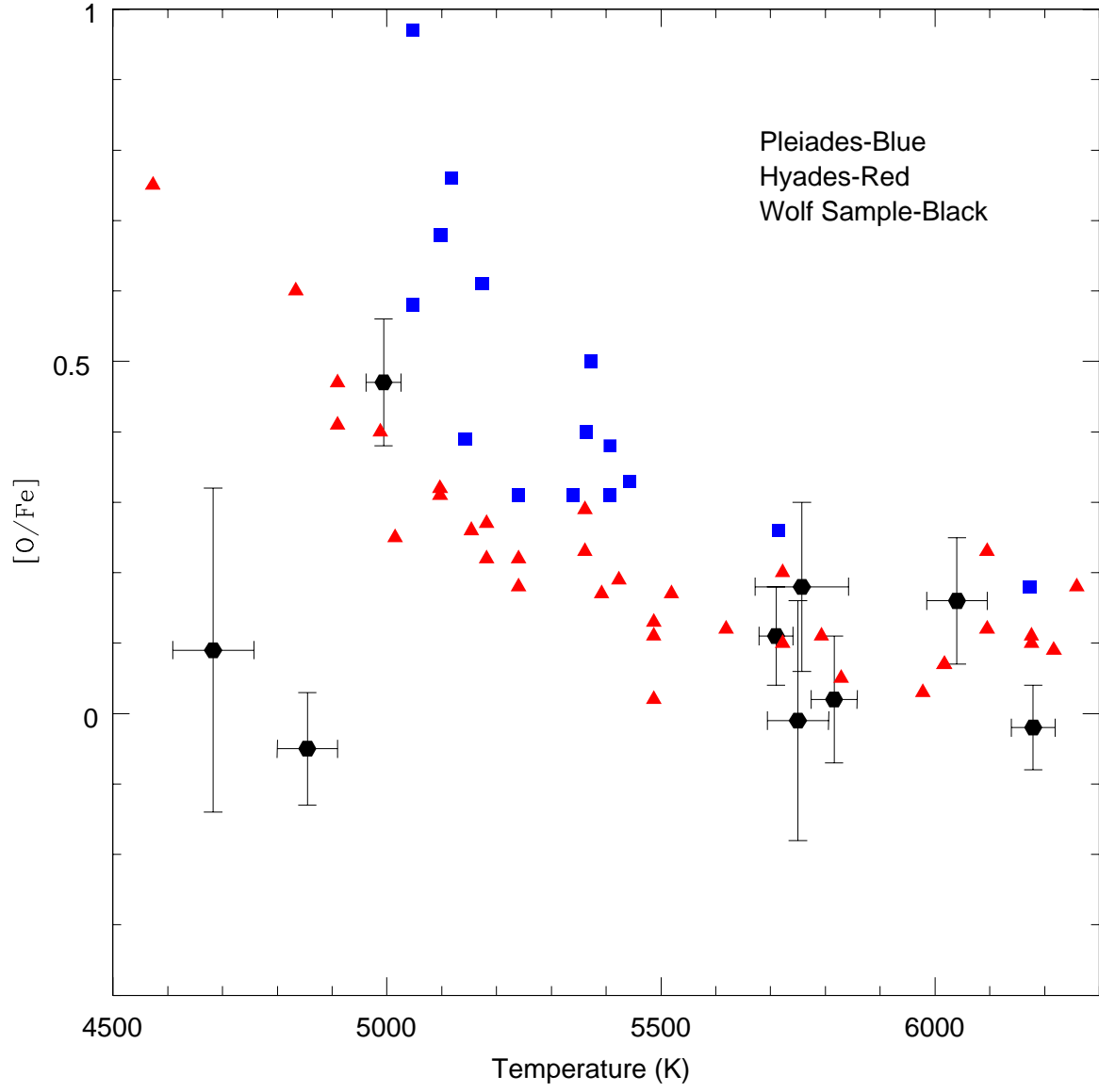


Fig. 12.— Oxygen abundances $[O/Fe]$ versus temperature for the Wolf 630 sample that were determined to be chemically homogeneous (black), the Pleiades (blue) and the Hyades (red).

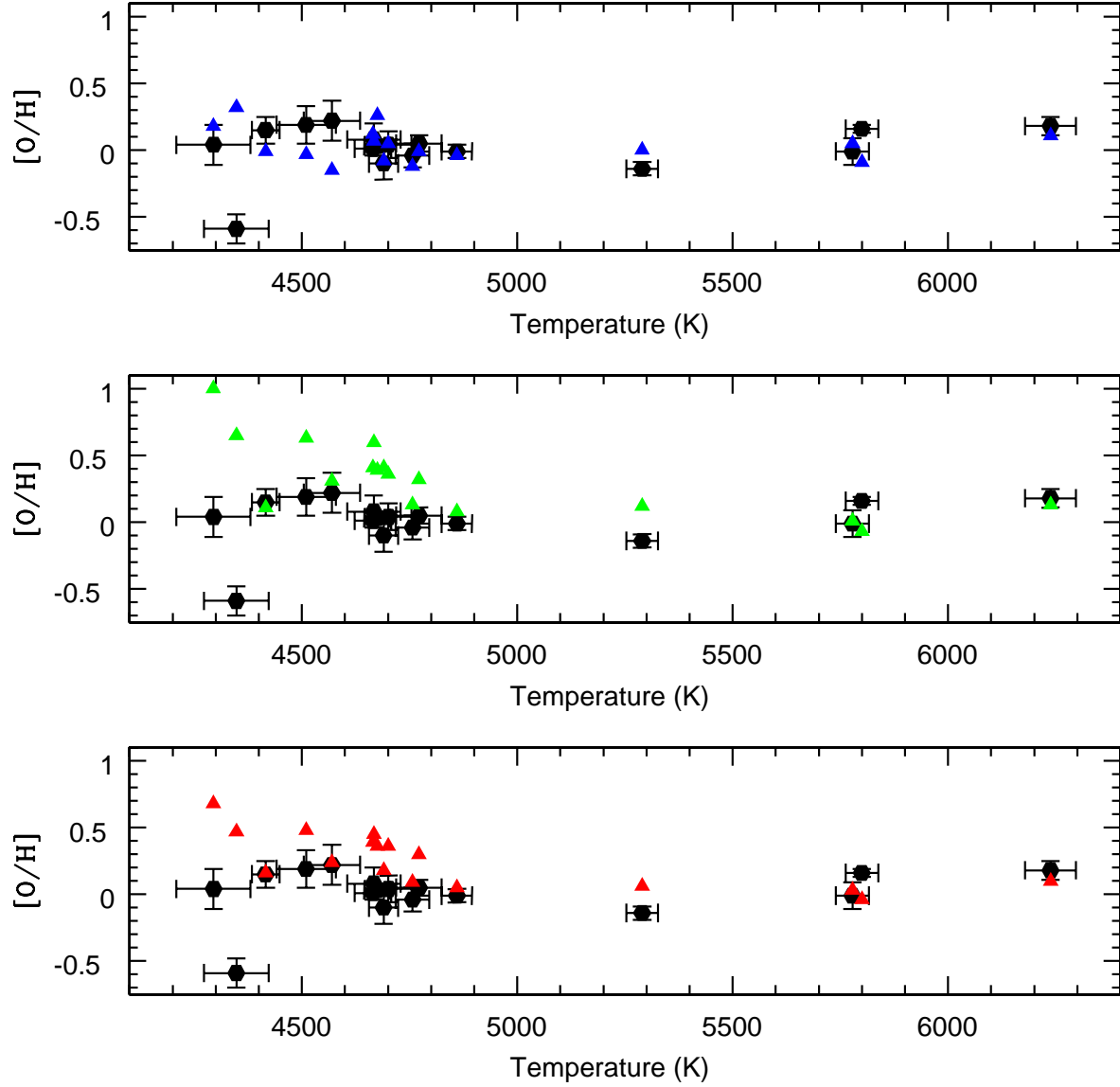


Fig. 13.— The $[O/H]$ abundance from the forbidden line (black hexagons) for subgiant and giant stars is plotted versus temperature in all windows. The top plot shows the NLTE $[O/H]$ abundances from the 7771 line of the triplet (blue triangles), the middle plot shows the NLTE $[O/H]$ from the 7774 line of the triplet (green triangles) and the bottom plot gives NLTE $[O/H]$ from the 7775 line (red triangles). The abundances derived from the 7771 line agree well, after NLTE corrections, with abundances from the forbidden line, but $[O/H]$ abundances from the redder lines of the triplet increase as a function of decreasing temperature.

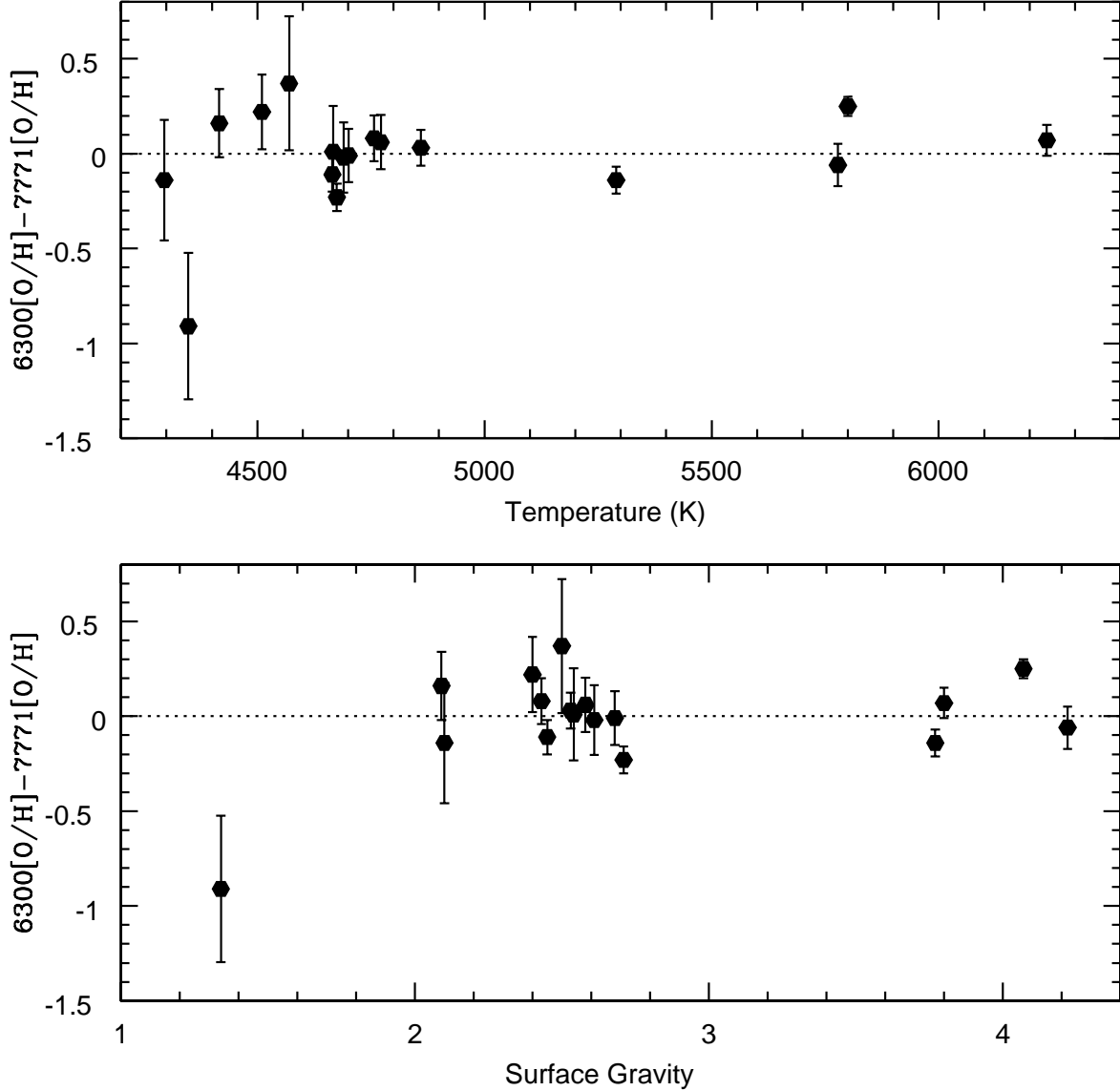


Fig. 14.— Differences in oxygen abundance between the forbidden line at 6300 Å and 7771 Å for the giant and subgiant stars. The NLTE corrected abundances from the triplet line generally agree with the 6300 forbidden line, with the exception of the metal weak cool star, HIP 114155. The clear agreement between the forbidden and the NLTE triplet abundance until reaching a low surface gravity possibly indicates that greater than expected NLTE effects impact the triplet abundances in more evolved stars.

Table 1. Kinematic Information

HIP	π (mas)	PM RA (mas/yr)	PM DEC (mas/yr)	Radial Velocity (kms ⁻¹)	U (kms ⁻¹)	V (kms ⁻¹)	W (kms ⁻¹)
102531	31.69 \pm 2.37	-6.10 \pm 2.88	-201.74 \pm 1.84	-7.0 \pm 0.9	16.6 \pm 1.6	-22.1 \pm 1.4	-14.1 \pm 1.3
102532	32.14 \pm 1.19	-25.88 \pm 1.33	-196.27 \pm 0.8	-6.5 \pm 0.9	17.8 \pm 0.9	-21.2 \pm 1.0	-11.3 \pm 0.6
103983	15.70 \pm 1.29	-71.25 \pm 1.53	-155.22 \pm 0.56	-6.8 \pm 2.0	35.2 \pm 3.4	-38.1 \pm 3.1	-3.8 \pm 1.1
104521	28.38 \pm 0.90	49.07 \pm 0.90	-151.85 \pm 0.64	-17.0 \pm 0.9	1.2 \pm 0.5	-29.0 \pm 0.9	-12.5 \pm 0.7
105341	61.04 \pm 1.31	-173.35 \pm 1.46	-721.75 \pm 0.72	21.1 \pm 2.0	38.9 \pm 1.4	-43.9 \pm 1.3	-18.2 \pm 1.3
11033	6.47 \pm 0.87	9.02 \pm 0.73	-58.12 \pm 0.57	-3.0 \pm 5.0	23.4 \pm 3.6	-36.2 \pm 4.9	-2.9 \pm 4.7
112222	24.86 \pm 0.93	9.80 \pm 10.66	-171.17 \pm 1.25	-2.0 \pm 5.0	15.1 \pm 0.9	-22.1 \pm 3.8	-18.9 \pm 3.4
112447	61.54 \pm 0.77	233.06 \pm 0.80	-492.04 \pm 0.61	-5.3 \pm 0.9	3.9 \pm 0.1	-31.6 \pm 0.8	-27.8 \pm 0.7
113622	5.96 \pm 0.80	5.06 \pm 1.28	-83.58 \pm 0.75	19.1 \pm 2.0	32.0 \pm 4.0	-36.7 \pm 6.7	-49.3 \pm 4.9
114155	6.07 \pm 0.67	0.20 \pm 0.56	-33.31 \pm 0.49	-26.8 \pm 0.9	14.9 \pm 1.5	-33.8 \pm 1.5	-5.6 \pm 2.3
114924	49.31 \pm 0.58	111.70 \pm 0.47	-236.29 \pm 0.44	-25.3 \pm 2.0	7.4 \pm 0.6	-27.3 \pm 1.9	-21.8 \pm 0.4
1170	6.62 \pm 0.82	-27.15 \pm 0.85	-73.78 \pm 0.41	-22.5 \pm 0.9	41.8 \pm 5.4	-40.5 \pm 4.5	17.1 \pm 1.1
12784	7.89 \pm 0.92	36.53 \pm 1.13	-35.79 \pm 0.7	-31.9 \pm 2.0	15.6 \pm 1.8	-39.0 \pm 3.5	14.1 \pm 1.4
13064	4.07 \pm 0.90	-2.07 \pm 0.99	-48.35 \pm 0.77	-14.0 \pm 5.0	42.8 \pm 8.3	-39.0 \pm 9.0	-4.7 \pm 5.7
13701	24.49 \pm 0.72	77.73 \pm 0.77	-219.99 \pm 0.63	-20.3 \pm 0.9	27.2 \pm 0.7	-40.3 \pm 1.2	9.5 \pm 0.8
14501	31.76 \pm 0.91	-7.99 \pm 1.05	-260.71 \pm 0.9	12.3 \pm 2.0	18.6 \pm 1.3	-29.6 \pm 0.9	-21.2 \pm 1.7
17792	4.61 \pm 1.01	72.36 \pm 1.10	10.28 \pm 0.89	-78.6 \pm 2.0	30.0 \pm 8.0	-42.5 \pm 9.0	95.5 \pm 11.5
23852	35.34 \pm 0.82	-5.61 \pm 0.91	-382.35 \pm 0.57	-23.8 \pm 2.0	39.5 \pm 1.9	-35.5 \pm 1.0	-19.6 \pm 0.9
29525	55.20 \pm 0.96	78.11 \pm 1.48	-297.1 \pm 0.77	3.0 \pm 5.0	5.9 \pm 4.7	-25.1 \pm 1.7	-6.4 \pm 0.3
29843	25.06 \pm 0.68	127.42 \pm 1.62	-258.64 \pm 0.5	-4.3 \pm 2.0	43.7 \pm 1.7	-32.6 \pm 1.8	4.4 \pm 0.6
32064	8.63 \pm 0.77	34.99 \pm 0.78	-46.05 \pm 0.6	0.9 \pm 0.9	18.9 \pm 1.8	-24.9 \pm 2.3	5.8 \pm 0.7
33671	21.26 \pm 0.74	0.60 \pm 0.83	-124.13 \pm 0.83	18.0 \pm 2.0	14.4 \pm 1.3	-25.7 \pm 1.8	-14.9 \pm 0.6

Table 1—Continued

HIP	π (mas)	PM RA (mas/yr)	PM DEC (mas/yr)	Radial Velocity (kms ⁻¹)	U (kms ⁻¹)	V (kms ⁻¹)	W (kms ⁻¹)
34440	10.68 ± 0.82	-5.02 ± 0.77	-103.52 ± 0.53	-17.0 ± 2.0	26.0 ± 2.0	-33.6 ± 3.1	-24.5 ± 1.7
3455	15.54 ± 0.82	-6.96 ± 0.88	-113.88 ± 0.6	0.6 ± 0.9	19.7 ± 1.1	-26.8 ± 1.5	-10.4 ± 1.0
34909	4.66 ± 0.90	14.66 ± 0.87	-41.8 ± 0.57	-9.2 ± 0.9	23.4 ± 3.0	-39.1 ± 8.2	-6.3 ± 1.2
3559	31.39 ± 1.03	-32.25 ± 0.99	-205.68 ± 0.59	-12.8 ± 2.0	21.9 ± 0.7	-25.7 ± 0.9	3.8 ± 1.9
36732	11.15 ± 0.70	24.10 ± 0.51	-70.23 ± 0.51	16.4 ± 2.0	16.0 ± 2.0	-31.3 ± 2.0	-5.5 ± 0.4
36962	13.57 ± 0.87	-39.58 ± 1.30	-108.08 ± 1.05	-20.6 ± 0.9	16.2 ± 0.9	-27.6 ± 2.1	-31.9 ± 1.7
3992	7.27 ± 0.79	22.13 ± 0.79	-63.64 ± 0.56	5.5 ± 2.0	5.8 ± 1.1	-35.5 ± 4.2	-25.8 ± 2.9
40023	23.82 ± 0.74	-71.82 ± 0.77	-348.06 ± 0.43	-43.0 ± 2.0	38.2 ± 1.7	-52.3 ± 2.0	-51.6 ± 1.4
41484	45.89 ± 0.84	-18.98 ± 1.14	-351.48 ± 0.66	-33.8 ± 2.0	21.3 ± 1.6	-38.3 ± 0.7	-23.3 ± 1.2
42499	53.98 ± 1.04	-109.35 ± 1.15	-499.89 ± 0.75	-13.4 ± 2.0	19.1 ± 1.5	-30.4 ± 1.2	-30.2 ± 1.1
4346	6.54 ± 1.00	-6.99 ± 0.99	-44.82 ± 0.58	1.9 ± 2.0	20.5 ± 3.3	-22.3 ± 3.6	-12.9 ± 2.5
43557	41.42 ± 1.19	153.13 ± 1.16	-235.45 ± 0.66	3.5 ± 0.9	19.5 ± 0.9	-25.5 ± 0.8	4.8 ± 0.5
45617	57.05 ± 1.08	49.78 ± 1.15	-507.62 ± 0.51	-18 ± 2.0	22.7 ± 1.4	-36.9 ± 0.9	-15.6 ± 1.4
48390	24.9 ± 0.82	20.98 ± 0.80	-174.56 ± 0.42	-1.8 ± 0.9	13.0 ± 0.7	-30.6 ± 1.1	-4. ± 0.7
5027	38.99 ± 1.88	-34.15 ± 1.75	-316.8 ± 1.4	2.8 ± 5.0	25.0 ± 1.3	-29.5 ± 1.4	-4.1 ± 5.0
50505	48.45 ± 0.85	62.98 ± 0.95	-299.34 ± 0.63	-8.3 ± 2.0	13.3 ± 1.2	-28.0 ± 0.5	1.2 ± 1.7
52366	4.39 ± 0.79	-3.18 ± 0.78	-18.84 ± 0.55	15.5 ± 0.9	-4.2 ± 1.0	-22.4 ± 3.7	12.2 ± 0.9
5286	48.2 ± 1.06	99.08 ± 1.03	-491.71 ± 0.55	-3.4 ± 2.0	9.4 ± 1.0	-34.4 ± 1.4	-34.3 ± 1.5
53229	33.4 ± 0.78	92.47 ± 0.69	-286.06 ± 0.55	16.1 ± 0.9	15.9 ± 0.7	-36.3 ± 0.8	22.6 ± 0.8
53465	10.46 ± 0.72	14.40 ± 0.71	-97.54 ± 0.54	-54.4 ± 2.0	41.1 ± 1.5	-43.4 ± 2.8	-37.2 ± 1.9
6108	11.41 ± 0.98	-5.54 ± 1.04	-37.51 ± 0.5	11.1 ± 5.0	9.5 ± 1.2	-11.3 ± 1.0	-12.4 ± 5.0
6732	10.63 ± 0.77	50.82 ± 1.03	-58.73 ± 0.61	-41.7 ± 2.0	12.2 ± 9.2	-51.3 ± 16.7	12.6 ± 19.7

Table 1—Continued

HIP	π	PM RA	PM DEC	Radial Velocity	U	V	W
	(mas)	(mas/yr)	(mas/yr)	(kms ⁻¹)	(kms ⁻¹)	(kms ⁻¹)	(kms ⁻¹)

Table 2. Solar Equivalent Widths

Wavelength Å	Ion	Excitation Potential eV	log(gf)	Equivalent Width mÅ
5505.881	Fe I	4.42	-1.30	54.7
5506.778	Fe I	0.99	-2.80	118.6
5522.447	Fe I	4.21	-1.55	41.4
5536.580	Fe I	2.83	-3.81	8.1
5539.280	Fe I	3.64	-2.66	17.5
5543.936	Fe I	4.22	-1.14	61.8
5546.500	Fe I	4.37	-1.31	49.9
5546.991	Fe I	4.22	-1.91	26.5
5553.578	Fe I	4.43	-1.41	58.9
5554.882	Fe I	4.55	-0.44	93.7
5557.977	Fe I	4.47	-1.28	61.9
5560.207	Fe I	4.43	-1.19	50.2
5562.706	Fe I	4.43	-0.64	56.8
5574.389	Fe I	4.42	-3.02	3.2
5576.089	Fe I	3.43	-1.00	111.0
5577.030	Fe I	5.03	-1.55	11.7
5579.335	Fe I	4.23	-2.40	9.0
5583.968	Fe I	4.19	-2.77	6.5
5587.574	Fe I	4.14	-1.85	33.4
5607.664	Fe I	4.15	-2.27	14.8
5617.186	Fe I	3.25	-2.88	35.6
5621.603	Fe I	5.11	-1.79	9.1
5646.684	Fe I	4.26	-2.50	7.2
5651.469	Fe I	4.47	-2.00	20.8
5652.318	Fe I	4.26	-1.95	23.1
5653.867	Fe I	4.39	-1.64	35.8
5661.346	Fe I	4.28	-1.74	22.4
5662.516	Fe I	4.18	-0.57	82.8
5667.518	Fe I	4.18	-1.58	49.2
5677.684	Fe I	4.10	-2.70	6.0

Table 2—Continued

Wavelength Å	Ion	Excitation Potential eV	log(gf)	Equivalent Width mÅ
5679.023	Fe I	4.65	-0.92	54.4
5680.240	Fe I	4.19	-2.58	9.3
5701.545	Fe I	2.56	-2.22	77.4
5705.981	Fe I	4.61	-0.53	91.1
5717.833	Fe I	4.28	-1.13	56.3
5724.454	Fe I	4.28	-2.64	7.3
5731.762	Fe I	4.26	-1.30	56.9
5732.275	Fe I	4.99	-1.56	14.3
5734.564	Fe I	4.96	-1.57	6.1
5739.986	Fe I	4.58	-2.06	6.7
5741.846	Fe I	4.26	-1.85	31.4
5752.032	Fe I	4.55	-1.18	53.2
5769.323	Fe I	4.61	-2.26	7.1
5775.081	Fe I	4.22	-1.30	56.6
5778.450	Fe I	2.59	-3.48	20.7
5902.474	Fe I	4.59	-1.81	13.0
5905.672	Fe I	4.65	-0.73	61.0
5916.247	Fe I	2.45	-2.99	52.6
5927.786	Fe I	4.65	-1.09	41.5
5929.667	Fe I	4.55	-1.41	37.1
5930.173	Fe I	4.65	-0.23	83.7
5933.792	Fe I	4.64	-2.23	8.2
5934.653	Fe I	3.93	-1.17	71.1
5956.690	Fe I	0.86	-4.60	52.7
5969.559	Fe I	4.28	-2.73	3.2
6003.010	Fe I	3.88	-1.12	81.4
6005.542	Fe I	2.59	-3.60	22.1
6015.243	Fe I	2.22	-4.68	5.2
6018.299	Fe I	4.65	-2.08	9.5
6027.051	Fe I	4.08	-1.09	64.5

Table 2—Continued

Wavelength Å	Ion	Excitation Potential eV	log(gf)	Equivalent Width mÅ
6034.033	Fe I	4.31	-2.42	9.5
6035.334	Fe I	4.29	-2.59	5.8
6054.072	Fe I	4.37	-2.31	8.7
6055.992	Fe I	4.73	-0.46	70.4
6065.482	Fe I	2.61	-1.53	113.7
6078.491	Fe I	4.80	-0.32	80.9
6078.999	Fe I	4.65	-1.12	44.6
6083.660	Fe I	3.88	-3.50	2.6
6085.259	Fe I	2.76	-3.10	41.5
6098.245	Fe I	4.56	-1.88	15.0
6102.171	Fe I	4.83	-0.52	76.4
6105.131	Fe I	4.55	-2.05	11.6
6120.249	Fe I	0.91	-5.96	5.5
6127.907	Fe I	4.14	-1.40	50.1
6151.617	Fe I	2.18	-3.30	48.8
6157.728	Fe I	4.08	-1.26	59.2
6159.368	Fe I	4.61	-1.97	12.4
6165.360	Fe I	4.14	-1.47	43.7
6170.504	Fe I	4.79	-0.44	76.4
6173.336	Fe I	2.22	-2.88	67.9
6187.987	Fe I	3.94	-1.72	48.1
6213.429	Fe I	2.22	-2.48	77.3
6219.280	Fe I	2.20	-2.43	91.5
6220.776	Fe I	3.88	-2.46	19.5
6226.730	Fe I	3.88	-2.22	29.2
6232.641	Fe I	3.65	-1.22	88.1
6240.645	Fe I	2.22	-3.23	50.3
6246.317	Fe I	3.60	-0.73	130.1
6252.554	Fe I	2.40	-1.69	116.5
6256.360	Fe I	2.45	-2.41	92.2

Table 2—Continued

Wavelength Å	Ion	Excitation Potential eV	log(gf)	Equivalent Width mÅ
6265.130	Fe I	2.17	-2.55	81.8
6271.280	Fe I	3.33	-2.72	22.7
6290.974	Fe I	4.73	-0.78	67.8
6293.924	Fe I	4.83	-1.72	13.0
6322.685	Fe I	2.59	-2.43	75.3
6335.328	Fe I	2.20	-2.18	96.6
6336.820	Fe I	3.68	-0.91	103.1
6344.148	Fe I	2.43	-2.92	58.2
6380.743	Fe I	4.19	-1.38	52.1
6392.538	Fe I	2.28	-4.03	17.0
6393.612	Fe I	2.43	-1.57	124.0
6408.018	Fe I	3.69	-1.02	90.8
6411.647	Fe I	3.65	-0.59	134.8
6469.193	Fe I	4.83	-0.77	62.1
6494.498	Fe I	4.73	-1.46	35.1
6494.980	Fe I	2.40	-1.27	138.6
6496.467	Fe I	4.79	-0.57	60.9
6498.945	Fe I	0.96	-4.70	44.0
6533.940	Fe I	4.56	-1.38	52.4
6574.228	Fe I	0.99	-5.02	26.7
6581.207	Fe I	1.49	-4.68	19.4
6584.575	Fe I	5.39	-1.34	3.7
6591.313	Fe I	4.59	-2.07	9.5
6592.913	Fe I	2.73	-1.47	110.2
6593.870	Fe I	2.43	-2.42	81.2
6597.557	Fe I	4.79	-1.07	46.5
6608.024	Fe I	2.28	-4.03	18.4
6609.110	Fe I	2.56	-2.69	66.9
6627.540	Fe I	4.55	-1.68	25.4
6646.932	Fe I	2.61	-3.99	10.2

Table 2—Continued

Wavelength Å	Ion	Excitation Potential eV	log(gf)	Equivalent Width mÅ
6653.850	Fe I	4.15	-2.52	9.9
6667.417	Fe I	2.45	-4.40	4.0
6667.711	Fe I	4.58	-2.11	7.8
6703.567	Fe I	2.76	-3.16	40.4
6704.481	Fe I	4.22	-2.66	6.9
6705.101	Fe I	4.61	-1.39	47.0
6710.316	Fe I	1.49	-4.88	16.5
6713.745	Fe I	4.79	-1.52	20.4
6715.383	Fe I	4.61	-1.64	28.7
6716.222	Fe I	4.58	-1.92	15.5
6725.353	Fe I	4.10	-2.30	17.8
6726.666	Fe I	4.61	-1.13	47.2
6732.065	Fe I	4.58	-2.21	8.1
6732.068	Fe I	4.58	-2.17	8.1
6733.151	Fe I	4.64	-1.58	26.7
6739.520	Fe I	1.56	-4.79	11.7
6745.090	Fe I	4.58	-2.16	8.8
6745.957	Fe I	4.08	-2.77	6.4
6746.953	Fe I	2.61	-4.35	4.0
6750.150	Fe I	2.42	-2.62	73.1
6752.716	Fe I	4.64	-1.30	35.5
6753.464	Fe I	4.56	-2.29	5.6
6777.408	Fe I	4.19	-2.82	7.9
6783.704	Fe I	2.59	-3.98	11.7
6786.856	Fe I	4.19	-2.07	24.0
6793.259	Fe I	4.08	-2.33	12.8
7114.549	Fe I	2.69	-4.01	7.9
7130.922	Fe I	4.22	-0.79	90.1
7142.517	Fe I	4.96	-0.82	34.1
7284.835	Fe I	4.14	-1.75	39.2

Table 2—Continued

Wavelength Å	Ion	Excitation Potential eV	log(gf)	Equivalent Width mÅ
7285.273	Fe I	4.61	-1.70	29.0
7802.473	Fe I	5.09	-1.52	16.3
7807.909	Fe I	4.99	-0.54	59.7
7820.803	Fe I	4.29	-2.64	5.4
7844.555	Fe I	4.83	-1.81	11.9
7879.748	Fe I	5.03	-1.65	25.8
5991.380	Fe II	3.15	-3.55	30.3
6084.110	Fe II	3.20	-3.80	21.7
6147.741	Fe II	3.89	-2.83	70.9
6149.249	Fe II	3.89	-2.88	35.7
6238.392	Fe II	3.89	-2.75	45.5
6247.557	Fe II	3.89	-2.44	51.8
6369.462	Fe II	2.89	-4.23	18.7
6416.919	Fe II	3.89	-2.88	41.3
6442.950	Fe II	5.55	-2.64	4.0
6446.400	Fe II	6.22	-2.11	4.2
6456.380	Fe II	3.90	-2.07	62.2
6300.310	O I	0.00	-9.72	5.2
6363.790	O I	0.00	-9.72	2.8
7771.940	O I	9.15	0.37	70.9
7774.170	O I	9.15	0.22	60.3
7775.390	O I	9.15	0.00	48.8
6154.230	Na I	2.10	-1.53	38.0
6160.750	Na I	2.10	-1.23	54.2
5711.090	Mg I	4.35	-1.83	102.5
6698.670	Al I	3.14	-1.95	22.1
7835.310	Al I	4.02	-0.47	43.4
7836.130	Al I	4.02	-0.31	57.0
5665.560	Si I	4.92	-1.94	39.9
5690.430	Si I	4.93	-1.77	52.0

Table 2—Continued

Wavelength Å	Ion	Excitation Potential eV	log(gf)	Equivalent Width mÅ
6142.480	Si I	5.62	-1.54	33.9
6145.010	Si I	5.62	-1.36	36.7
6155.130	Si I	5.62	-0.78	84.7
5868.570	Ca I	2.93	-1.57	2.7
6161.297	Ca I	2.52	-1.27	61.8
6166.439	Ca I	2.52	-1.14	69.6
6169.040	Ca I	2.52	-0.79	95.9
6169.560	Ca I	2.53	-0.47	107.1
6455.600	Ca I	2.52	-1.50	59.7
6464.680	Ca I	2.52	-2.53	15.5
6499.650	Ca I	2.52	-1.00	86.8
6572.800	Ca I	0.00	-4.28	33.7
5877.657	Ti I	3.32	-0.08	15.5
5978.541	Ti I	1.87	-0.50	20.9
5999.658	Ti I	2.24	-1.48	11.3
6064.626	Ti I	1.05	-1.94	10.3
6126.216	Ti I	1.07	-1.43	22.6
6258.102	Ti I	1.44	-0.35	49.7
6258.706	Ti I	1.46	-0.24	70.8
6261.098	Ti I	1.43	-0.48	49.6
6336.099	Ti I	1.44	-1.74	6.7
6668.376	Ti I	3.58	0.20	4.7
6743.122	Ti I	0.90	-1.63	17.6
7138.906	Ti I	1.44	-1.70	6.4
7357.727	Ti I	1.44	-1.12	23.9
6214.600	Ti II	2.04	-3.46	7.1
6491.561	Ti II	2.06	-1.79	43.8
6491.582	Ti II	2.06	-2.15	44.6
6513.045	Ti II	4.00	-1.31	3.2
6606.949	Ti II	2.06	-2.79	8.9

Table 2—Continued

Wavelength Å	Ion	Excitation Potential eV	log(gf)	Equivalent Width mÅ
6606.949	Ti II	2.06	-2.79	9.5
7355.438	Ti II	2.59	-1.91	15.2
7355.438	Ti II	2.59	-1.91	17.6
6330.100	Cr I	0.94	-2.99	26.9
6729.750	Cr I	4.39	-0.66	4.2
6013.530	Mn I	3.07	-0.25	86.8
6016.670	Mn I	3.08	-0.10	95.8
6021.800	Mn I	3.08	0.03	98.8
5846.990	Ni I	1.68	-3.21	23.6
6086.280	Ni I	4.26	-0.51	44.2
6175.370	Ni I	4.09	-0.53	47.8
6327.600	Ni I	1.68	-3.23	38.3
6378.260	Ni I	4.15	-1.00	32.5
6414.590	Ni I	4.15	-1.18	15.6
6482.810	Ni I	1.93	-2.97	42.5
6532.880	Ni I	1.93	-3.47	17.1
6598.610	Ni I	4.23	-1.02	26.9
6635.140	Ni I	4.42	-0.82	26.2
6643.640	Ni I	1.68	-2.01	92.6
6767.780	Ni I	1.83	-1.89	80.4
6772.320	Ni I	3.66	-0.98	51.3
6842.040	Ni I	3.66	-1.48	23.8
5853.690	Ba II	0.60	-1.00	66.2
6141.730	Ba II	0.70	-0.07	119.6
6496.910	Ba II	0.60	-0.41	100.0

Table 3. Basic Physical Parameters

HIP	T_{spec} K	$\text{Log}(g)$ cms^{-2}	χ kms^{-1}	[Fe/H]
102531	6238 ± 59	3.80 ± 0.16	1.85 ± 0.05	0.07 ± 0.04
103983	5750 ± 56	4.52 ± 0.20	1.16 ± 0.06	0.02 ± 0.05
105341 ^a	4005 ± 88	4.67 ± 0.28	0.83 ± 0.60	-0.05 ± 0.19
11033	4510 ± 69	2.40 ± 0.30	1.60 ± 0.08	0.12 ± 0.04
112222	6369 ± 100	4.10 ± 0.26	1.69 ± 0.08	0.04 ± 0.07
112447	6095 ± 100	3.75 ± 0.25	1.82 ± 0.16	-0.34 ± 0.08
113622	4295 ± 86	2.10 ± 0.25	1.52 ± 0.13	0.00 ± 0.08
114155 ^a	4348 ± 75	1.34 ± 0.25	2.19 ± 0.08	-0.58 ± 0.07
114924	6179 ± 40	4.36 ± 0.12	1.59 ± 0.05	0.06 ± 0.03
12784	4701 ± 54	2.68 ± 0.07	1.49 ± 0.10	0.09 ± 0.13
13701	4675 ± 30	2.71 ± 0.07	1.37 ± 0.08	-0.03 ± 0.03
14501	5785 ± 57	4.44 ± 0.20	1.24 ± 0.03	-0.08 ± 0.04
17792	4416 ± 32	2.09 ± 0.20	1.50 ± 0.03	-0.52 ± 0.06
23852	5778 ± 38	4.22 ± 0.23	1.22 ± 0.06	-0.14 ± 0.06
29525	5710 ± 31	4.57 ± 0.08	1.28 ± 0.09	-0.03 ± 0.03
29843	6130 ± 60	4.11 ± 0.15	1.52 ± 0.08	0.12 ± 0.08
33671	6040 ± 55	4.40 ± 0.15	1.38 ± 0.08	-0.21 ± 0.04
34440	4757 ± 39	2.43 ± 0.21	1.46 ± 0.08	-0.15 ± 0.04
3455	4860 ± 35	2.53 ± 0.07	1.49 ± 0.05	0.00 ± 0.03
3559	5800 ± 38	4.07 ± 0.05	1.27 ± 0.05	-0.18 ± 0.03
36732	4667 ± 62	2.54 ± 0.20	1.44 ± 0.09	0.10 ± 0.06
3992	4772 ± 53	2.58 ± 0.13	1.59 ± 0.06	-0.15 ± 0.04
40023	5290 ± 37	3.77 ± 0.06	1.21 ± 0.06	-0.05 ± 0.03
41484	5855 ± 39	4.41 ± 0.15	1.17 ± 0.05	0.08 ± 0.03
42499	4994 ± 32	4.41 ± 0.20	0.59 ± 0.19	-0.56 ± 0.10
4346 ^a	3820 ± 200	1.39 ± 0.30	1.33 ± 0.17	0.24 ± 0.18
43557	5816 ± 42	4.52 ± 0.10	1.15 ± 0.12	-0.03 ± 0.04
45617	4855 ± 55	4.35 ± 0.10	1.01 ± 0.10	-0.12 ± 0.02
5027 ^b	4398 ± 79	4.70 ± 0.29	0.00 ± 0.30	-0.08 ± 0.17
50505	5655 ± 41	4.42 ± 0.14	1.16 ± 0.10	-0.14 ± 0.03

^a Surface gravities for these stars are physical, calculated as discussed in the test.

^b Surface gravity for this star is physical, calculated as discussed in the text. The microturbulence was set to 0.

Table 3—Continued

HIP	T _{spec} K	Log(g) cms ⁻²	χ kms ⁻¹	[Fe/H]
5286	4683 ± 74	4.56 ± 0.25	0.54 ± 0.24	0.29 ± 0.07
53229	4690 ± 34	2.61 ± 0.20	1.47 ± 0.05	-0.10 ± 0.15
53465	4570 ± 65	2.50 ± 0.30	1.30 ± 0.08	-0.08 ± 0.07
6732	4665 ± 42	2.45 ± 0.10	1.58 ± 0.06	-0.03 ± 0.04

Table 4. All Equivalent Widths

Wavelength Å	Ion	Excitation Potential eV	log(gf)	HIP102531 EQW mÅ	HIP102531 LogN(x)	HIP105341 EQW mÅ	HIP105341 LogN(x)	HIP105341 LogN(x) Error
6154.230	Na I	2.10	-1.53	42.70	6.31	125.00	5.83	
6160.750	Na I	2.10	-1.23	60.00	6.24	
5711.090	Mg I	4.35	-1.83	104.30	7.60	129.20	7.64	
6698.670	Al I	3.14	-1.95	74.80	6.64	
7835.310	Al I	4.02	-0.47	46.80	6.24	73.80	6.16	
7836.130	Al I	4.02	-0.31	58.40	6.23	
5665.560	Si I	4.92	-1.94	44.90	7.58	
5690.430	Si I	4.93	-1.77	52.50	7.53	
6142.480	Si I	5.62	-1.54	54
6145.010	Si I	5.62	-1.36	37.90	7.49	
6155.130	Si I	5.62	-0.78	84.40	7.52	25.50	7.87	
5868.570	Ca I	2.93	-1.57	
6161.297	Ca I	2.52	-1.27	
6166.439	Ca I	2.52	-1.14	70.90	6.30	
6169.040	Ca I	2.52	-0.79	
6169.560	Ca I	2.53	-0.47	
6455.600	Ca I	2.52	-1.50	55.60	6.40	135.80	5.93	
6464.680	Ca I	2.52	-2.53	15.10	6.58	
6499.650	Ca I	2.52	-1.00	88.30	6.42	
6572.800	Ca I	0.00	-4.28	36.70	6.35	
5877.657	Ti I	3.32	-0.08	53.00	5.49	
5978.541	Ti I	1.87	-0.50	24.60	4.90	92.90	4.60	

Table 4—Continued

Wavelength Å	Ion	Excitation Potential eV	log(gf)	HIP102531 EQW mÅ	HIP102531 LogN(x)	HIP105341 EQW mÅ	HIP105341 LogN(x)	HIP105341 LogN(x) F
5999.658	Ti I	2.24	-1.48	49.20	5.41	
6064.626	Ti I	1.05	-1.94	11.20	5.10	96.80	5.01	
6126.216	Ti I	1.07	-1.43	25.10	5.04	106.40	4.64	
6258.102	Ti I	1.44	-0.35	55.40	4.91	
6258.706	Ti I	1.46	-0.24	74.60	5.18	
6261.098	Ti I	1.43	-0.48	49.10	4.92	194.90	4.84	
6336.099	Ti I	1.44	-1.74	73.20	4.97	
6668.376	Ti I	3.58	0.20	14.30	4.74	
6743.122	Ti I	0.90	-1.63	5.2...	
7138.906	Ti I	1.44	-1.70	
7357.727	Ti I	1.44	-1.12	
6214.600	Ti II	2.04	-3.46	
6491.561	Ti II	2.06	-1.79	38.40	4.87	57.70	6.24	
6513.045	Ti II	4.00	-1.31	1.60	4.56	7.90	6.87	
6606.949	Ti II	2.06	-2.79	12.70	5.19	
7355.438	Ti II	2.59	-1.91	
7355.438	Ti II	2.59	-1.91	
6330.100	Cr I	0.94	-2.99	25.90	5.67	
6729.750	Cr I	4.39	-0.66	
6013.530	Mn I	3.07	-0.25	86.60	5.62	
6016.670	Mn I	3.08	-0.10	96.00	5.63	163.30	5.53	
6021.800	Mn I	3.08	0.03	101.90	5.59	

Table 4—Continued

Wavelength Å	Ion	Excitation Potential eV	log(gf)	HIP102531 EQW mÅ	HIP102531 LogN(x)	HIP105341 EQW mÅ	HIP105341 LogN(x)	HIP105341 LogN(x)
5846.990	Ni I	1.68	-3.21	51.80	6.33	
6086.280	Ni I	4.26	-0.51	42.20	6.24	38.10	6.71	
6175.370	Ni I	4.09	-0.53	50.90	6.26	
6327.600	Ni I	1.68	-3.23	37.10	6.33	81.10	6.81	
6378.260	Ni I	4.15	-1.00	31.30	6.39	
6414.590	Ni I	4.15	-1.18	
6482.810	Ni I	1.93	-2.97	74.80	6.78	
6532.880	Ni I	1.93	-3.47	34.50	6.56	
6598.610	Ni I	4.23	-1.02	29.50	6.44	96.00	6.93	
6635.140	Ni I	4.42	-0.82	21.90	6.24	16.30	6.72	
6643.640	Ni I	1.68	-2.01	92.00	6.13	123.90	6.07	
6767.780	Ni I	1.83	-1.89	
6772.320	Ni I	3.66	-0.98	46.30	6.18	
6842.040	Ni I	3.66	-1.48	
5853.690	Ba II	0.60	-1.00	
6141.730	Ba II	0.70	-0.07	133.80	2.53	
6496.910	Ba II	0.60	-0.41	

Table 5. Abundances

HIP	[Mg/H]	[Si/H]	[Ca/H]	[Ti/H]	[Ti2/H]	[Cr/H]	[Mn/H]	[Ni/H]	[Na/H]
102531	0.13 ± 0.08	0.16 ± 0.08	0.08 ± 0.06	0.07 ± 0.08	0.01 ± 0.08	-0.02 ± 0.09	-0.14 ± 0.05	0.05 ± 0.05	0.18 ± 0.03
103983	-0.04 ± 0.09	0.02 ± 0.06	0.06 ± 0.08	0.03 ± 0.09	-0.06 ± 0.26	-0.06 ± 0.11	-0.25 ± 0.17	-0.02 ± 0.08	0.05 ± 0.05
105341	0.00 ± 0.12	-0.17 ± 0.15	-0.20 ± 0.12
11033	0.24 ± 0.12	0.40 ± 0.13	0.13 ± 0.14	0.04 ± 0.17	...	-0.01 ± 0.10	...	0.23 ± 0.19	0.23 ± 0.18
112222	0.11 ± 0.11	0.04 ± 0.10	0.10 ± 0.08	0.06 ± 0.09	-0.01 ± 0.12	-0.01 ± 0.13	-0.25 ± 0.09	0.05 ± 0.13	0.16 ± 0.12
112447	-0.21 ± 0.12	-0.24 ± 0.17	0.17 ± 0.07	-0.24 ± 0.15	-0.41 ± 0.11	-0.35 ± 0.15	-0.75 ± 0.15	-0.28 ± 0.14	-0.23 ± 0.11
113622	0.18 ± 0.13	-0.01 ± 0.09	0.09 ± 0.14	0.04 ± 0.17	...	0.03 ± 0.19	0.03 ± 0.20	0.22 ± 0.26	...
114155	-0.51 ± 0.24	...	-0.61 ± 0.20	-0.62 ± 0.09	-0.62 ± 0.14	-0.05 ± 0.08
114924	0.17 ± 0.10	0.10 ± 0.06	0.06 ± 0.05	0.08 ± 0.13	...	0.21 ± 0.07	-0.18 ± 0.09	0.06 ± 0.06	0.20 ± 0.12
12784	0.28 ± 0.12	0.04 ± 0.04	0.04 ± 0.15	0.18 ± 0.20	...	-0.02 ± 0.14	0.24 ± 0.09	0.16 ± 0.22	0.18 ± 0.12
13701	0.11 ± 0.09	0.07 ± 0.12	0.12 ± 0.12	-0.01 ± 0.11	-0.11 ± 0.08	-0.11 ± 0.05	-0.02 ± 0.11	-0.04 ± 0.10	-0.05 ± 0.12
14501	0.06 ± 0.11	-0.13 ± 0.15	...	0.01 ± 0.10	-0.05 ± 0.11	-0.11 ± 0.11	-0.31 ± 0.07	-0.12 ± 0.08	-0.01 ± 0.09
17792	-0.12 ± 0.08	-0.28 ± 0.16	0.16 ± 0.12	-0.15 ± 0.11	-0.24 ± 0.10	-0.60 ± 0.05	-0.54 ± 0.11	-0.44 ± 0.14	...
23852	0.03 ± 0.08	-0.04 ± 0.03	0.03 ± 0.10	-0.03 ± 0.08	0.11 ± 0.05	-0.20 ± 0.08	-0.44 ± 0.09	-0.19 ± 0.06	-0.21 ± 0.03
29525	-0.05 ± 0.07	-0.06 ± 0.06	0.06 ± 0.07	-0.06 ± 0.08	-0.08 ± 0.07	0.03 ± 0.07	-0.14 ± 0.05	-0.09 ± 0.04	-0.10 ± 0.04
29843	0.13 ± 0.07	0.12 ± 0.04	0.04 ± 0.08	0.03 ± 0.09	0.09 ± 0.06	0.09 ± 0.09	0.03 ± 0.07	0.11 ± 0.09	0.16 ± 0.06
33671	-0.13 ± 0.08	-0.17 ± 0.04	0.04 ± 0.08	-0.18 ± 0.08	-0.25 ± 0.14	-0.33 ± 0.07	-0.61 ± 0.08	-0.27 ± 0.12	-0.25 ± 0.05
34440	0.09 ± 0.08	0.01 ± 0.08	0.08 ± 0.12	-0.20 ± 0.09	-0.06 ± 0.14	-0.31 ± 0.05	-0.05 ± 0.08	-0.11 ± 0.08	-0.02 ± 0.04
3455	0.17 ± 0.20	-0.13 ± 0.14	0.14 ± 0.10	0.00 ± 0.09	-0.06 ± 0.17	-0.04 ± 0.20	0.00 ± 0.09	0.04 ± 0.09	0.20 ± 0.20
3559	-0.10 ± 0.07	-0.16 ± 0.03	0.03 ± 0.07	-0.12 ± 0.09	-0.18 ± 0.07	-0.29 ± 0.07	-0.50 ± 0.04	-0.24 ± 0.09	-0.29 ± 0.06
36732	0.30 ± 0.11	0.06 ± 0.21	0.21 ± 0.10	-0.02 ± 0.24	...	-0.03 ± 0.15	0.28 ± 0.11	0.29 ± 0.10	0.24 ± 0.13
3992	-0.01 ± 0.10	-0.07 ± 0.13	0.13 ± 0.11	-0.15 ± 0.15	-0.02 ± 0.11	-0.18 ± 0.12	-0.17 ± 0.08	-0.11 ± 0.09	0.07 ± 0.08

Table 5—Continued

HIP	[Mg/H]	[Si/H]	[Ca/H]	[Ti/H]	[Ti2/H]	[Cr/H]	[Mn/H]	[Ni/H]	[Na/H]
40023	-0.01 ± 0.07	0.02 ± 0.09	0.09 ± 0.12	0.00 ± 0.13	0.04 ± 0.08	-0.08 ± 0.08	-0.13 ± 0.07	-0.10 ± 0.07	0.00 ± 0.05
41484	0.04 ± 0.07	0.04 ± 0.02	0.02 ± 0.05	0.05 ± 0.06	-0.01 ± 0.04	...	0.00 ± 0.06	0.00 ± 0.05	0.05 ± 0.04
42499	-0.14 ± 0.13	-0.37 ± 0.08	0.08 ± 0.14	-0.26 ± 0.06	-0.15 ± 0.12	-0.61 ± 0.03	-0.72 ± 0.06	-0.77 ± 0.11	-0.42 ± 0.14
4346	0.30 ± 0.15	0.80 ± 0.20	0.20 ± 0.14	0.43 ± 0.22	...	0.44 ± 0.11	0.45 ± 0.14	0.54 ± 0.23	0.36 ± 0.16
43557	-0.08 ± 0.06	-0.05 ± 0.05	0.05 ± 0.08	-0.03 ± 0.10	-0.07 ± 0.09	-0.08 ± 0.07	-0.19 ± 0.06	-0.10 ± 0.06	-0.07 ± 0.04
45617	-0.17 ± 0.10	-0.28 ± 0.10	0.10 ± 0.16	-0.13 ± 0.22	...	-0.13 ± 0.10	-0.17 ± 0.07	-0.24 ± 0.09	-0.09 ± 0.11
5027	-0.23 ± 0.10	-0.20 ± 0.20	0.20 ± 0.18	-0.06 ± 0.17	0.09 ± 0.17	...	-0.26 ± 0.11	-0.18 ± 0.07	-0.41 ± 0.14
50505	-0.06 ± 0.08	-0.16 ± 0.04	0.04 ± 0.08	-0.07 ± 0.09	0.00 ± 0.09	-0.18 ± 0.09	-0.26 ± 0.07	-0.21 ± 0.10	-0.16 ± 0.03
5286	0.27 ± 0.10	0.25 ± 0.11	0.11 ± 0.19	0.27 ± 0.15	0.37 ± 0.00	0.39 ± 0.19	0.18 ± 0.11	0.31 ± 0.10	0.26 ± 0.12
53229	-0.04 ± 0.09	-0.01 ± 0.20	0.20 ± 0.07	-0.15 ± 0.10	-0.03 ± 0.08	-0.28 ± 0.10	-0.11 ± 0.13	0.01 ± 0.18	0.07 ± 0.08
53465	0.13 ± 0.11	0.00 ± 0.19	0.19 ± 0.22	-0.10 ± 0.22	0.22 ± 0.09	-0.14 ± 0.09	-0.05 ± 0.19	0.01 ± 0.13	-0.01 ± 0.14
6732	0.10 ± 0.10	-0.10 ± 0.14	0.14 ± 0.13	-0.01 ± 0.12	...	-0.10 ± 0.12	0.04 ± 0.10	0.03 ± 0.13	0.02 ± 0.10

Table 6. Sample Abundance Sensitivity for $[\text{Fe}/\text{H}]$

Star	Parameter	Abundance Sensitivity
HIP3455	$\Delta T = \pm 150$	∓ 0.02
	$\Delta \log g = \pm 0.12$	∓ 0.01
	$\Delta \zeta = \pm 0.60$	± 0.02
	$\Delta \langle [\text{Fe}/\text{H}] \rangle$	± 0.01
	Total Uncertainty in $[\text{Fe}/\text{H}]$	± 0.03
HIP3559	$\Delta T = \pm 150$	∓ 0.03
	$\Delta \log g = \pm 0.12$	∓ 0.00
	$\Delta \zeta = \pm 0.60$	± 0.01
	$\Delta \langle [\text{Fe}/\text{H}] \rangle$	± 0.01
	Total Uncertainty in $[\text{Fe}/\text{H}]$	± 0.03
HIP103983	$\Delta T = \pm 150$	∓ 0.04
	$\Delta \log g = \pm 0.12$	∓ 0.02
	$\Delta \zeta = \pm 0.60$	± 0.01
	$\Delta \langle [\text{Fe}/\text{H}] \rangle$	± 0.01
	Total Uncertainty in $[\text{Fe}/\text{H}]$	± 0.05

Table 7. Oxygen Abundances

HIP	EW ₇₇₇₁ mÅ	EW ₇₇₇₄ mÅ	EW ₇₇₇₅ mÅ	LTE [O/H] ₇₇₇₁	LTE [O/H] ₇₇₇₄	LTE [O/H] ₇₇₇₅	[O/H] ₆₃₀₀	NLTE [O/H] ₇₇₇₁	NLTE [O/H] ₇₇₇₄
102531	157.7	139.7	114.0	0.48 ± 0.04	0.44 ± 0.04	0.33 ± 0.05	0.18 ± 0.07	0.11 ± 0.04	0.13 ± 0.04
103983	67.8	60.8	48.0	-0.03 ± 0.09	0.00 ± 0.09	0.01 ± 0.11	...	0.00 ± 0.09	0.01 ± 0.09
11033	23.0	37.8	27.1	-0.06 ± 0.14	0.62 ± 0.15	0.48 ± 0.14	0.19 ± 0.14	-0.03 ± 0.14	0.63 ± 0.15
112222	129.8	117.5	101.0	0.16 ± 0.09	0.18 ± 0.09	0.17 ± 0.14	...	-0.05 ± 0.09	-0.02 ± 0.09
112447	109.1	96.3	76.6	0.01 ± 0.09	0.01 ± 0.09	-0.06 ± 0.11	...	-0.02 ± 0.09	-0.14 ± 0.09
113622	19.5	45.4	26.5	0.15 ± 0.28	1.06 ± 0.28	0.69 ± 0.29	0.04 ± 0.15	0.18 ± 0.28	1.00 ± 0.28
114155	44.2	52.0	35.3	0.39 ± 0.37	0.75 ± 0.37	0.53 ± 0.18	-0.59 ± 0.11	0.32 ± 0.37	0.65 ± 0.37
114924	109.2	97.6	78.2	0.11 ± 0.03	0.14 ± 0.03	0.08 ± 0.04	...	0.03 ± 0.03	0.07 ± 0.03
12784	31.4	36.5	29.9	0.02 ± 0.10	0.35 ± 0.10	0.35 ± 0.10	0.04 ± 0.10	0.05 ± 0.10	0.36 ± 0.10
13701	36.3	34.8	27.9	0.24 ± 0.06	0.37 ± 0.06	0.35 ± 0.06	0.03 ± 0.04	0.26 ± 0.06	0.39 ± 0.06
14501	75.0	71.9	55.8	0.06 ± 0.07	0.16 ± 0.07	0.11 ± 0.07	...	0.05 ± 0.07	0.14 ± 0.07
17792	22.9	21.7	18.2	-0.03 ± 0.15	0.09 ± 0.15	0.15 ± 0.15	0.15 ± 0.10	-0.01 ± 0.15	0.11 ± 0.15
23852	80.8	66.3	55.4	0.09 ± 0.05	0.04 ± 0.05	0.06 ± 0.07	-0.01 ± 0.10	0.05 ± 0.05	0.01 ± 0.05
29525	66.8	59.8	47.4	0.01 ± 0.04	0.07 ± 0.04	0.06 ± 0.04	...	0.04 ± 0.04	0.10 ± 0.04
29843	121.8	104.1	85.2	0.27 ± 0.06	0.22 ± 0.06	0.17 ± 0.06	...	0.11 ± 0.06	0.10 ± 0.06
33671	86.7	78.8	62.6	-0.05 ± 0.05	0.01 ± 0.05	-0.02 ± 0.05	...	-0.08 ± 0.05	-0.02 ± 0.05
34440	36.7	40.3	31.4	-0.09 ± 0.08	0.18 ± 0.14	0.13 ± 0.11	-0.04 ± 0.09	-0.12 ± 0.08	0.13 ± 0.14
3455	45.4	44.1	34.7	0.01 ± 0.08	0.14 ± 0.08	0.10 ± 0.08	-0.01 ± 0.05	-0.04 ± 0.08	0.08 ± 0.08
3559	77.1	66.8	56.1	-0.04 ± 0.04	-0.03 ± 0.04	0.00 ± 0.04	0.16 ± 0.03	-0.09 ± 0.04	-0.07 ± 0.04
36732	33.9	47.6	34.6	0.06 ± 0.21	0.61 ± 0.20	0.46 ± 0.22	0.08 ± 0.12	0.07 ± 0.21	0.60 ± 0.20
3992	39.3	46.5	37.6	0.02 ± 0.13	0.38 ± 0.13	0.35 ± 0.12	0.05 ± 0.06	-0.01 ± 0.13	0.32 ± 0.13
40023	50.8	48.7	36.2	0.00 ± 0.05	0.13 ± 0.05	0.06 ± 0.04	-0.14 ± 0.05	0.00 ± 0.05	0.12 ± 0.05

Table 7—Continued

HIP	EW ₇₇₇₁ mÅ	EW ₇₇₇₄ mÅ	EW ₇₇₇₅ mÅ	LTE [O/H] ₇₇₇₁	LTE [O/H] ₇₇₇₄	LTE [O/H] ₇₇₇₅	[O/H] ₆₃₀₀	NLTE [O/H] ₇₇₇₁	NLTE [O/H] ₇₇₇₄
42499	21.2	17.7	13.5	-0.18 ± 0.05	-0.16 ± 0.05	-0.13 ± 0.05	...	-0.09 ± 0.05	-0.08 ± 0.05
4346	-0.10 ± 0.16
43557	72.4	62.9	47.3	-0.01 ± 0.05	0.01 ± 0.05	-0.05 ± 0.06	...	0.00 ± 0.05	0.01 ± 0.05
45617	11.8	14.3	8.9	-0.26 ± 0.08	-0.06 ± 0.09	-0.17 ± 0.08	...	-0.17 ± 0.08	0.02 ± 0.09
5286	16.6	18.0	13.0	0.27 ± 0.23	0.50 ± 0.23	0.46 ± 0.23	...	0.38 ± 0.23	0.60 ± 0.23
53229	28.2	39.3	26.4	-0.11 ± 0.14	0.40 ± 0.15	0.17 ± 0.13	-0.10 ± 0.12	-0.08 ± 0.14	0.41 ± 0.15
53465	22.5	30.8	23.5	-0.19 ± 0.32	0.29 ± 0.33	0.23 ± 0.33	0.22 ± 0.15	-0.15 ± 0.32	0.31 ± 0.33
6732	37.9	42.3	34.4	0.12 ± 0.09	0.41 ± 0.09	0.40 ± 0.11	0.01 ± 0.01	0.12 ± 0.09	0.41 ± 0.09

Table 8. Lithium

HIP	LogN(Li)
3559	2.45 ± 0.03
5027	≤ -0.20
5286	≤ 0.70
14501	≤ 0.30
23852	2.00 ± 0.04
29525	2.03 ± 0.02
29843	≤ 1.60
33671	2.61 ± 0.05
41484	1.93 ± 0.04
42499	≤ 1.09
43557	≤ 1.50
45617	≤ 0.60
50505	≤ 0.50
102531	1.90 ± 0.07
103983	1.90 ± 0.07
105341	≤ -0.25
112447	2.30 ± 0.07
114924	2.75 ± 0.06
112222	≤ 1.22

Table 9. Membership Status

HIP	T_{spec} K	[Fe/H]
UNLIKELY		
3559	5800 ± 38	-0.18 ± 0.03
4346*	3820 ± 200	0.24 ± 0.18
5027**	4398 ± 79	-0.08 ± 0.17
5286	4683 ± 74	0.29 ± 0.07
11033	4510 ± 69	0.12 ± 0.04
17792	4416 ± 32	-0.52 ± 0.06
23852	5778 ± 38	-0.14 ± 0.06
29843	6130 ± 60	0.12 ± 0.08
33671	6040 ± 55	-0.21 ± 0.04
42499	4994 ± 32	-0.56 ± 0.10
45617	4855 ± 55	-0.12 ± 0.02
50505	5655 ± 41	-0.14 ± 0.03
103983	5750 ± 56	0.02 ± 0.05
112447	6095 ± 100	-0.34 ± 0.08
114155*	4348 ± 75	-0.58 ± 0.07
POSSIBLE		
3992	4772 ± 53	-0.15 ± 0.04
12784	4701 ± 54	0.09 ± 0.13
34440	4757 ± 39	-0.15 ± 0.04
36732	4667 ± 62	0.10 ± 0.06
41484	5855 ± 39	0.08 ± 0.03
53229	4690 ± 34	-0.10 ± 0.15
105341*	4005 ± 88	-0.05 ± 0.19
114924	6179 ± 40	0.06 ± 0.03
PROBABLE		
3455	4860 ± 35	0.00 ± 0.03
6732	4665 ± 42	-0.03 ± 0.04

A. Notes on Individual Stars: Unlikely Members

A.1. HIP 3559: $T=5800$ $\log g=4.07$ $\xi=1.27$ $[\text{Fe}/\text{H}]=-0.18$

This star resides above the ZAMS in the HR diagram. Ca II H and K measurements indicate an inactive chromosphere ($\log R'_{HK}=-5.16$); the activity-age calibrations of Mamajek & Hillenbrand (2008) suggest an age of 9.4 ± 2.7 Gyr, indicating the HR diagram position is not a result of being a PMS star. Indeed, Holmberg et al. (2007) derive an isochrone age, from Padova isochrones (Girardi et al. (2000), Salasnich et al. (2000)), of 7.6 Gyr; again, clearly not PMS. Fitting the position of this star using Yale-Yonsei isochrones (Demarque et al. 2004), it appears to lie near the turnoff for a 6.8 ± 0.4 Gyr isochrone. In addition, our spectroscopic surface gravity ($\log g \approx 4.07$) is consistent with subgiant status. In order to determine if the lithium abundance ($\log N(\text{Li})=2.45$) is consistent with a subgiant abundance, we obtain a reasonable estimate of the initial lithium abundance as a ZAMS dwarf and then compare the inferred lithium dilution with theoretical calculations. If the star is a 6.8 Gyr subgiant, Yale-Yonsei isochrones yield a mass of $1.10 \pm 0.2 M_{\odot}$. Assuming this mass, as a ZAMS star of Pleiades age (≈ 120 Myr), HIP 3559 would have had a main-sequence temperature of 6158 K. From the lithium abundance trend traced by the Pleiades (6), we infer that this star would have possessed an abundance of $\log N(\text{Li}) \sim 3.00$ as a 6158 K ZAMS star. Assuming this as the ZAMS lithium, the observed dilution of ~ 0.55 dex is consistent with predicted lithium dilution calculations for a $1.11 M_{\odot}$ at an age of ~ 6.8 Gyr, performed using the Clemson-American University of Beirut stellar evolution code. HIP3559 is therefore removed from consideration as a member of a 2-3 Gyr Wolf group. Instead, it is assumed that this is an ~ 7.0 Gyr subgiant.

A.2. HIP 4346: $T=3820$ $\log g=1.39$ $\xi=1.33$ $[\text{Fe}/\text{H}]=0.24$

The metallicity of $[\text{Fe}/\text{H}]=0.24 \pm 0.18$ is high compared to the near zero modal value of our sample and rests outside of the abundance band for the full sample. While the uncertainty in our $[\text{Fe}/\text{H}]$ value is substantial, this star is clearly metal rich across all elements. Considering this clear metal richness across all abundances, this star is considered an unlikely member of a dominant chemical group comprised by our sample.

Table 9—Continued

HIP	T_{spec} K	[Fe/H]
13701	4675 ± 30	-0.03 ± 0.03
14501	5785 ± 57	-0.08 ± 0.04
29525	5710 ± 31	-0.03 ± 0.03
40023	5290 ± 37	-0.05 ± 0.03
43557	5816 ± 42	-0.03 ± 0.04
53465	4570 ± 65	-0.08 ± 0.07
102531	6238 ± 59	0.07 ± 0.04
112222	6369 ± 100	0.04 ± 0.07
113622	4295 ± 86	0.00 ± 0.08

Table 10. Group Abundances

Element	[X/H]	$\chi^2_{\nu all}$	$\chi^2_{\nu group}$	$\chi^2_{\nu probable}$
Al/H	-0.01 ± 0.01	4.71	2.46	2.96
Ba/H	0.00 ± 0.02	3.82	1.12	1.60
Ca/H	0.09 ± 0.02	0.42	0.45	0.13
Cr/H	-0.10 ± 0.02	12.54	2.78	0.43
Fe/H	-0.01 ± 0.01	10.40	2.77	1.06
Mg/H	0.04 ± 0.02	2.12	1.60	1.11
Mn/H	-0.11 ± 0.02	10.39	2.67	1.59
Na/H	0.02 ± 0.01	7.46	4.70	4.97
Ni/H	-0.03 ± 0.02	4.09	1.92	1.31
Si/H	0.02 ± 0.02	4.82	0.77	0.84
Ti/H	-0.01 ± 0.02	1.46	0.67	0.21
Ti2/H	-0.01 ± 0.02	2.72	0.77	1.28

A.3. HIP 5027: $T=4398$ $\log g=4.70$ $\xi=0.00$ $[\text{Fe}/\text{H}]=-0.08$

Hip 5027 has an Fe abundance which is consistent with the dominant $[\text{Fe}/\text{H}]$ values exhibited by our sample. However, the abundances of other elements (Na, Al, Mn, Ni, Mg and Si) are all markedly sub-solar, and rest outside of the abundance bands for the full sample. The lithium upper limit of $\log N(\text{Li}) \leq -0.20$ may place the star in the trend traced by the Pleiades (Figure 6); however the significant spread in the Pleiades lithium abundances as a function of decreasing temperature makes a firm conclusion regarding age difficult to draw. With the majority of elements disagreeing with the dominant abundance trends of the entire sample, this star is classified as an unlikely member of a chemically dominant group.

A.4. HIP 5286: $T=4683$ $\log g=4.56$ $\xi=0.54$ $[\text{Fe}/\text{H}]=0.29$

HIP 5286 is a member of the high metallicity “bump” at $[\text{Fe}/\text{H}]=\sim 0.30$ in Figure 3. In examining the HR diagram, HIP 5286 rests above the main sequence. The lithium upper limit of $\log N(\text{Li}) \leq 0.70$ places the star below the Pleiades trend, suggesting that it is not a young, PMS star. Coincidence with the other open cluster trends is uncertain as the literature lithium abundances do not extend to sufficiently cool temperatures, indicating the need for lithium abundance determinations in cool stars in intermediate age open clusters. Examining the abundances of other elements, HIP 5286 is clearly a metal rich star with $[\text{Fe}/\text{H}]=0.29 \pm 0.07$, well outside of the dominant abundance bands. This star as an unlikely member of a chemically dominant group.

A.5. HIP 11033: $T=4510$ $\log g=2.40$ $\xi=1.60$ $[\text{Fe}/\text{H}]=0.12$

The metallicity of HIP 11033 ($[\text{Fe}/\text{H}] = 0.12 \pm 0.04$) places this star outside of the $[\text{Fe}/\text{H}]$ band used to constrain homogeneity in abundance. In examining abundances for other elements, this star is seen to reside outside of the homogeneous bands for Al, Mg and Si and it barely resides inside the band for Na. While the other elements are within the abundance band, it is due primarily to the significant uncertainties associated with the respective abundances. With a metallicity that is inconsistent with homogeneity and considering that half of the remaining abundances are inconsistent with the sample, this is considered to be an unlikely member of a chemically homogeneous group.

A.6. HIP 17792: T=4416 logg=2.09 ξ =1.50 [Fe/H]=-0.52

HIP 17792, with $[\text{Fe}/\text{H}] = -0.52 \pm 0.06$, is one of the stars comprised by the low metallicity bump in Figure 3. This low metallicity extends across all the Fe peak elements. The high Al abundance ($[\text{Al}/\text{Fe}] = 0.40$) is of note in that this star shows similar large enhancements to those seen in red giants in some open cluster (Schuler et al. (2009)). The consistently low abundances of Fe, Fe peak elements and most α elements lead to the conclusion that this star is an unlikely candidate that is part of a dominant chemical subsample.

A.7. HIP 23852: T=5778 logg=4.22 ξ =1.22 [Fe/H]=-0.14

This star resides above the ZAMS, raising the question of pre-main sequence or subgiant status. An isochrone age of 8.8 Gyr was estimated from Padova isochrones by Nordström et al. (2004). Using Yonsei-Yale isochrones, we find an age of 7.9 ± 0.10 Gyr. Our spectroscopic surface gravity of the star, $\log g = 4.22$, is consistent with a super ZAMS classification. Using a stellar mass of $1.08 M_{\odot}$, inferred from the Yale-Yonsei isochrones, the ZAMS temperature of this star would have been 6052 K. The ZAMS lithium abundance, inferred from the Pleiades trend of Figure 6, $\log N(\text{Li}) = 3.00$, suggests a factor of 10 lithium depletion, consistent with theoretical calculations. The current lithium abundance of $\log N(\text{Li}) = 2.00$ is too low for a PMS star, and appears consistent with the M67 Li- T_{eff} trend, which implies the star is an ~ 5 Gyr dwarf or mildly evolved subgiant. The metallicity lays outside of the abundance band used for judging homogeneity of the sample. The Fe peak elements, Na, Al and Ba all reside outside of the dominant abundance bands. This star is, therefore, not considered a member of a dominant chemical subsample of 2-3 Gyr in age.

A.8. HIP 33671: T=6040 logg=4.40 ξ =1.38 [Fe/H]=-0.21

The metallicity of HIP 33671 is $[\text{Fe}/\text{H}] = -0.21 \pm 0.04$. This places the star well outside of the apparent dominant metallicity band. The metal poor nature applies across all other elements, with the star not resting within any abundance bands. While its Li abundance is not inconsistent with 2-3 Gyr age (Figure 6), HIP 33671 is unlikely to be part of a dominant chemical subsample.

A.9. HIP 42499: T=4994 logg=4.41 ξ =0.59 [Fe/H]=-0.56

HIP 42499 is a member of the metal-weak peak in the full sample [Fe/H] distribution (Figure 3). A Li upper limit of $\log N(\text{Li}) \leq 1.09$ potentially places this star in the Hyades trend, however the chromospheric activity ($\log R'_{HK} = -4.98$) is much lower than the activity trend for the Hyades, suggesting it is older than the Hyades. With an $[\text{Fe}/\text{H}] = -0.56 \pm 0.10$ and consistent metal deficiency evinced across all elements, this star is classified as an unlikely member of a chemically dominant group.

A.10. HIP45617 T=4855 logg=4.35 ξ =1.01 [Fe/H]=-0.12

This star resides above the lower main sequence. The lithium upper limit ($\log N(\text{Li}) \leq 0.60$) shows that the star is not a pre-main sequence object. The activity of $\log R'_{HK} = -4.60$, from the Ca II H and K survey of the solar neighborhood of D. Soderblom (private communication), would place the star below the activity trend of the Hyades, qualitatively suggesting that a Hyades age would be a reasonable lower limit. However, the spectroscopic surface gravity is somewhat low for a dwarf star. A possible explanation is that overionization, observed in many cool cluster dwarfs (Schuler et al. (2003)), is yielding spuriously low surface gravities. With a greater number of atoms in ionized states, the gravity would have to be artificially lowered to obtain ionization balance. However excellent agreement is seen between the spectroscopic gravity ($\log g = 4.35$) and the physical gravity ($\log g = 4.38$). The star's $[\text{Fe}/\text{H}] = -0.12 \pm 0.02$ is inconsistent with it being a member of the dominant metallicity distribution and, it does not reside within the abundance bands for any other elements. While its low surface gravity remains a mystery, we consider HIP 45617 an unlikely member of a dominant chemical group.

A.11. HIP 50505: T=5655 logg=4.42 ξ =1.16 [Fe/H]=-0.14

This star clearly resides on the main sequence, with a low Li upper limit of $\log N(\text{Li}) \leq 0.50$, consistent with the star being an old (\leq M67 age) dwarf. The star is clearly metal poor ($[\text{Fe}/\text{H}] = -0.14 \pm 0.03$) when compared with our sample mean metallicity. In examining all other elements, the star rests outside of the group abundance bands for Fe, the Fe peak elements and for Si. The tightly constrained metallicity and the consistently low abundances across all Fe peak elements lead to classification of this star as an unlikely group member of a dominant metallicity group in our sample.

A.12. HIP 112447: T=6095 logg=3.75 ξ =1.82 [Fe/H]=-0.34

This star has a distinctly low $[\text{Fe}/\text{H}]=-0.34 \pm 0.08$, making it a member of the metal poor peak of Figure 3. The abundances of other elements are similarly metal poor. With this strong evidence for metal poverty, HIP 112447 is classified as an unlikely member of a chemically dominant group.

A.13. HIP 114155: T=4348 logg=1.34 ξ =2.19 [Fe/H]=-0.58

The $[\text{Fe}/\text{H}]$ of HIP 114155 is clearly low $[\text{Fe}/\text{H}]=-0.58 \pm 0.07$. This giant shows similarly low abundances of all elements with the exception of $[\text{Na}/\text{H}]$ and $[\text{Al}/\text{H}]$. The enhanced Na and Al abundance ratios ($[\text{Na}/\text{Fe}]=0.53 \pm 0.08$ and $[\text{Al}/\text{Fe}]=0.51 \pm 0.11$) can be compared with those in open cluster giants. In a recent analysis of Hyades dwarfs and giants, Schuler et al. (2009) found enhancements in Na and Al of between 0.20 and 0.50 dex in cluster giants compared with dwarfs, a result in conflict with standard stellar models. Similar abundance enhancements are seen in other open clusters (Jacobson et al. 2007). This points to a pattern of anomalously large Na and Al abundances in population I giants, likely a side effect of NLTE effects, discussed in more detail below. Regardless, the distinctly low metal abundances across multiple elements suggest that HIP114155 is an unlikely member of the dominant chemical group in our sample.

B. Notes on Individual Stars: Possible Members

B.1. HIP 3992: T=4772 logg=2.58 ξ =1.59 [Fe/H]=-0.15

HIP 3992 has an $[\text{Fe}/\text{H}]=-0.15 \pm 0.04$. This places it outside of the Fe band that appears to dominate the sample. However, all other abundances rest inside their respective bands, suggesting the star is chemically consistent with the overall dominant chemical composition of our sample. We thus consider HIP 3992 a possible member of a dominant chemical group in our sample.

B.2. HIP 12784: T=4701 logg=2.68 ξ =1.49 [Fe/H]=0.09

The uncertainty associated with the metallicity of HIP 12784 ($[\text{Fe}/\text{H}]=0.09 \pm 0.13$) places it within the dominant Fe band. The star resides outside of the abundance bands for

Mn, Mg, Al, Na and Ni. Thus we consider this star only a possible member of a dominant chemical group.

B.3. HIP 29843: $T=6130$ $\log g=4.11$ $\xi=1.52$ $[\text{Fe}/\text{H}]=0.12$

HIP 29843 has a Li upper limit of $\log N(\text{Li}) \leq 1.60$. We estimate a Yale-Yonsei isochrone mass of $1.43 \pm 0.02 M_{\odot}$. Using this mass to determine the ZAMS temperature of the star yields $T_{\text{ZAMS}}=6678$ K. This temperature, when compared to Figure 6, would have placed this star in or on the blue-edge of the lithium dip while a dwarf. Currently, as a subgiant that has emerged from the lithium dip, the lack of lithium suggests that the deepening convection zone in the subgiant has not brought lithium back to the surface. This appears consistent with the findings of Balachandran (1990) who also inferred little transport of lithium to the surface in subgiants emerging from the lithium dip in M67. The metallicity of the star ($[\text{Fe}/\text{H}]=0.12 \pm 0.08$) appears to be somewhat high compared to the peak of the sample, and, indeed it rests outside of the $[\text{Fe}/\text{H}]$ band. This star also resides outside of the abundance bands for Si, Na, Cr and Mn. However, it rests within the abundance bands for the other seven elements. This leads us to consider HIP 29843 to be a possible member of a dominant metallicity sample.

B.4. HIP 34440: $T=4757$ $\log g=2.43$ $\xi=1.46$ $[\text{Fe}/\text{H}]=-0.15$

Fe, Ti and Cr for this star lay outside of the respective abundance bands. The other elements all reside within their bands, consistent with homogeneity. We consider this star only a possible member of a dominant homogeneous chemical group in our sample.

B.5. HIP 36732: $T=4667$ $\log g=2.54$ $\xi=1.44$ $[\text{Fe}/\text{H}]=0.10$

Fe, Mn, Ni, Na and Mg all appear slightly enriched when compared to the dominant abundance bands. While the other elements have abundances within their respective bands the consistent overabundances for Fe, Mn, Ni, Na and Mg suggest this star be classified as only a possible member of a chemically dominant subsample.

B.6. HIP 41484: $T=5855$ $\log g=4.41$ $\xi=1.17$ $[\text{Fe}/\text{H}]=0.08$

The Fe abundance of HIP 41484 ($[\text{Fe}/\text{H}]=0.08 \pm 0.03$) is supersolar compared to our sample mean. This supersolar value, however, is not consistent across the other elements. The abundances derived for all other elements agree with the abundance bands used to constrain homogeneity. The lithium abundance of $\log N(\text{Li})=1.93 \pm 0.04$ places the star below the lithium trend of the Pleiades and suggests a lower age limit of approximately Hyades age, and perhaps at least as large as the age of NGC 752 and M67. Considering the homogeneity across multiple elements, but not for Fe, this star is considered a possible member of a chemically homogeneous dominant 2-3 Gyr subsample.

B.7. HIP 43557: $T=5816$ $\log g=4.52$ $\xi=1.15$ $[\text{Fe}/\text{H}]=-0.03$

The $[\text{Fe}/\text{H}]$ of HIP 43557 matches the mean abundance of our entire sample. Mg, Na and Si however, do not appear to lay within their respective abundance bands. The average abundances for Ti, Ti II, Cr and Ba all rest near the sample mean abundances irrespective of their uncertainties, suggesting a high degree of homogeneity. In examining the lithium abundance, the star rests below the 5 Gyr trend in the Li- T_{eff} relation, perhaps suggesting an older age. Although the $[\text{Fe}/\text{H}]$ agrees well with the mean metallicity and the average abundances of multiple elements are close to the respective mean abundances for the group, the evidence from Mg, Na and Si and the lower lithium abundance make HIP 43557 a possible group member.

B.8. HIP103983: $T=5750$ $\log g=4.52$ $\xi=1.16$ $[\text{Fe}/\text{H}]=0.02$

The status of this star is somewhat of an enigma. While an isochrone fit is consistent with placement on the subgiant branch of an 8.5 ± 0.11 Gyr isochrone, the surface gravity of $\log g=4.52$ suggests a dwarf luminosity class. Note the significant uncertainty in the surface gravity measurement (0.20 dex). Valenti & Fischer (2005) find a surface gravity of 4.37, consistent with the lower limit of the spectroscopic gravity derived here. Further comparing surface gravity estimates, the physical surface gravity derived for this star is $\log g=4.22 \pm 0.23$, which would be consistent with subgiant status. The lithium abundance, $\log N(\text{Li})=1.90 \pm 0.07$ places this star within the lower end of the lithium trend observed in both NGC 752 and M67. This would suggest consistency with a 2-3 Gyr age for a dwarf, but definitive age conclusions based on the lithium are impractical considering the scatter and overlap in lithium abundances in both NGC 752 and M67. If the star were indeed a

subgiant, does the lithium abundance yield different conclusions? The mass of an 8.5 Gyr subgiant with a temperature of 5750 K would be $1.05 M_{\odot}$. This yields a ZAMS temperature, $T_{ZAMS}=5754$ K, which coincides with a Pleiades lithium abundance of $\log N(\text{Li})=3.00$ on the so-called “lithium plateau”. Assuming this as a reasonable ZAMS lithium abundance, this star would have ≈ 1.10 dex depletion, which is not entirely consistent with predictions of 0.20-0.90 dex of lithium dilution for a $1 M_{\odot}$ obtained from the Clemson-American University of Beirut Stellar Evolution Code. This perhaps points to the star not being a clear subgiant, however, the evolutionary status of this star remains uncertain. Examining the abundances, the star has an $[\text{Fe}/\text{H}]=0.02 \pm 0.05$, which is consistent with it being a member of a chemically dominant subgroup with a characteristic metallicity near -0.03. The α and Fe peak elements, likewise, yield abundances that reside within the respective abundance bands that are used to characterize homogeneity. Considering the uncertainties in the surface gravities and the potential that the lithium abundance negates a subgiant classification and that the abundances are homogeneous with the rest of the sample, we consider this star a possible member of a chemically homogeneous sub-group.

B.8.1. HIP 105341: $T=4005$ $\log g=4.67$ $\xi=0.83$ $[\text{Fe}/\text{H}]=-0.05$

This star is the coolest dwarf in the sample. The chromospheric activity ($\log R'_{HK}=-4.552$) from Gray et al. (2006) suggests this is a relatively active star, which may be consistent with PMS status, although it is not inconsistent with a main sequence age. The activity derived age, using the updated age-activity relation of Mamajek & Hillenbrand (2008) is $0.85 \text{ Gyr} \pm 0.25 \text{ Gyr}$, which places the star on the main sequence, in agreement with the surface gravity. While this age estimate suggests the star does not belong in a 2-3 Gyr Wolf group, the quoted error only includes uncertainty based in the calibration relationship. Furthermore, activity based ages, while useful in a statistically significant sample size, may not be robust enough to constrain individual field star ages well enough to eliminate pre-main sequence status for this star, although the surface gravity may suggest this is not a pre-main sequence object. The lithium upper limit ($\log N(\text{Li}) \leq -0.25$) may plausibly place the star in the lithium trend traced by the Pleiades in Figure 6, but without lithium abundances for more cool Pleiads the picture is unclear. The Fe abundance of the star ($[\text{Fe}/\text{H}]=-0.05 \pm 0.19$) is consistent with membership in a dominant chemical group centered on $[\text{Fe}/\text{H}]=-0.03$. It also resides within the abundance bands for all elements with measurable abundances (Mg, Ti and Al). Although the chemical homogeneity of this star is constrained by all available abundances, this star is considered only a possible member of a chemically dominant 2-3 Gyr group due to the lack of abundances across all elements.

B.9. HIP 114924: $T=6179$ $\log g=4.36$ $\xi=1.59$ $[\text{Fe}/\text{H}]=0.06$

With $[\text{Fe}/\text{H}]=0.06 \pm 0.03$, HIP114924 resides outside of the dominant Fe band. It also appears to reside outside of the bands for Cr and Na. However, it resides inside the bands for all other elements. The lithium abundance, $\log N(\text{Li})=2.75 \pm 0.06$ places the star along the lower envelope of the so-called lithium plateau in Figure 6. This would suggest that HIP114924 is a good preserver of lithium. It is below the Hyades plateau and falls on the NGC752 trend, therefore a 2-3 Gyr age is quite consistent with the Li. Given that Fe, Cr and Na are not consistent with our samples modal values, but that other elements are, this star is considered only a possible member of the chemically dominant group.

C. Note on Individual Stars: Likely Members

C.1. HIP 3455: $T=4860$ $\log g=2.53$ $\xi=1.49$ $[\text{Fe}/\text{H}]=0.00$

This star has an $[\text{Fe}/\text{H}]=0.00 \pm 0.03$ that is consistent with the dominant group metallicity. In examining the other elements, it resides within every abundance band, suggesting its classification as a likely member of a homogeneous subsample.

C.2. HIP 6732: $T=4665$ $\log g=2.45$ $\xi=1.58$ $[\text{Fe}/\text{H}]=-0.03$

This star has a metallicity ($[\text{Fe}/\text{H}]=-0.03 \pm 0.04$) which matches closely with the weighted average of our sample. Examining the other elements, the abundances all appear to reside within the respective group metallicity bands. The homogeneity demonstrated across all elements and the agreement of $[\text{Fe}/\text{H}]$ with the mean group abundance suggest that HIP 6732 is a likely member of a chemically dominant subsample.

C.3. HIP 13701: $T=4675$ $\log g=2.71$ $\xi=1.37$ $[\text{Fe}/\text{H}]=-0.03$

This star clearly resides within the dominant $[\text{Fe}/\text{H}]$ band. Indeed, its abundance is nearly identical to the weighted mean of the sample. It appears consistent with the metallicity bands for all elements. This homogeneity with the rest of the sample leads to classifying HIP 13701 as a likely group member.

C.4. HIP 14501: T=5785 logg=4.44 ξ =1.24 [Fe/H]=-0.08

Having [Fe/H]=-0.08 \pm 0.04, HIP 14501 resides inside of the dominant metallicity band. In fact, it resides in the metallicity bands for all elements and, in many cases, the average abundance of each element nearly matches with the weighted mean used to characterize the abundance trend of the sample. The upper limit lithium abundance ($\log N(\text{Li}) \leq 0.30$), however, perhaps suggests an age of much greater than 2-3 Gyr. We note this inconsistency, but based on the chemical abundances of all other elements, this star is considered a likely member.

C.5. HIP 29525: T=5710 logg=4.57 ξ =1.28 [Fe/H]=-0.03

This star resides on the main sequence of the isochrones in Figure 7. The lithium abundance ($\log N(\text{Li})=2.03 \pm 0.02$) places the star within the abundance trends traced by NGC 752 and M67, perhaps consistent with membership in a 2-3 Gyr group. The metallicity ([Fe/H]=-0.03 \pm 0.03) firmly places this star within the abundance band that dominates the sample. The abundances of Na and Al are outside of their respective abundance bands but all other elements are within the bands. We consider this a candidate for likely membership in a chemically homogeneous and dominant subsample of 2-3 Gyr age.

C.6. HIP 40023: T=5290 logg=3.77 ξ =1.21 [Fe/H]=-0.05

HIP 40023 has an [Fe/H]=-0.05, which is within the metallicity band of the sample. Indeed, its abundances across multiple elements fit inside the respective metallicity bands. The small spread in abundances for the star itself and relative to the overall sample abundance bands, lead to classification of this star as a likely member of a dominant chemically homogeneous 2-3 Gyr subsample.

C.7. HIP 53229: T=4690 logg=2.61 ξ =1.47 [Fe/H]=-0.10

The Fe abundance of HIP 53229 ([Fe/H]=-0.10 \pm 0.15) is consistent with the mean abundance band of our sample. Examining the other abundances, Cr is the only element that does not appear within the abundance band for the group sample. Homogeneity is observed across all the other elements, therefore this star is likely a member of a chemically homogeneous subgroup.

C.8. HIP 53465: T=4570 logg=2.50 ξ =1.30 [Fe/H]=-0.08

The metallicity of HIP 53465 ($[\text{Fe}/\text{H}]=-0.08 \pm 0.07$) is consistent with this star being a member of the dominant chemical subgroup. While abundances of Al and Ti II are found to lay outside of the sample abundance bands, the remaining elements show a high degree of homogeneity. For most elements, the abundances lay within the abundance band. Thus, this star is considered a likely member of a chemically dominant group in our sample.

C.9. HIP 102531: T=6238 logg=3.80 ξ =1.85 [Fe/H]=0.07

The metallicity of HIP 102531 ($[\text{Fe}/\text{H}]=0.07 \pm 0.04$) is barely outside of the $3\text{-}\sigma$ cutoff of the mean Fe abundance of the whole sample. However, this star resides within the mean abundance bands of Al, Ba, Ca, Mg, Mn, Ni, Si, Ti and Ti 2. In Figure 6, this is the warmest sample star that has lithium, and can be seen to lay significantly beneath any trend traced by any of the plotted open cluster dwarf abundances. From the HR diagram, this star lies along the early subgiant branch of a 2.7 Gyr isochrone, which indicates a mass of $1.5 \pm 0.1 M_{\odot}$. In comparing this star with Figure 11 of Balachandran (1995), who plot lithium abundances for open clusters versus stellar mass, the lithium abundance for the derived mass appears to be between the trends for M67 and NGC 752, consistent with the estimated isochrone age of 2.7 Gyr. This would suggest that the star has suffered subgiant and/or main sequence Lithium dip depletion. Recognizing that the majority of elements suggest this star is part of a chemically homogeneous subsample, and the ~ 3 Gyr age implied by isochrones and Li, it is classified as a likely member of a dominant subsample.

C.10. HIP 112222: T=6369 logg=4.10 ξ =1.69 [Fe/H]=0.04

HIP 112222, with $[\text{Fe}/\text{H}]=0.04 \pm 0.07$, rests within the dominant Fe band and the abundance bands for every other element with the exception of Mn. HIP112222 is located at the turnoff of a 2.7 Gyr isochrone in Figure 7. The position along this isochrone implies a mass of $\sim 1.3 M_{\odot}$ consistent with this possibly being a lithium dip star, providing an explanation for the apparently low upper limit lithium abundance of $\log N(\text{Li}) \leq 1.22$. Its placement in homogeneous abundance bands across multiple elements and apparent 2-3 Gyr isochrone age lead to this star being considered a likely member of the dominant subsample.

C.11. HIP 113622: T=4295 logg=2.10 ξ =1.52 [Fe/H]=0.00

With $[\text{Fe}/\text{H}]=0.00 \pm 0.08$, this star rests comfortably inside the dominant Fe band. The Ni abundance of $[\text{Ni}/\text{H}]=0.29$ is uncharacteristically high for our sample, but the uncertainty of 0.26 dex is significant, which can bring the star into close agreement with the Ni band. Furthermore, HIP 113622 is consistently within the metallicity bands for all other elements. Consequently, it is classified as a likely member of a dominant subsample.

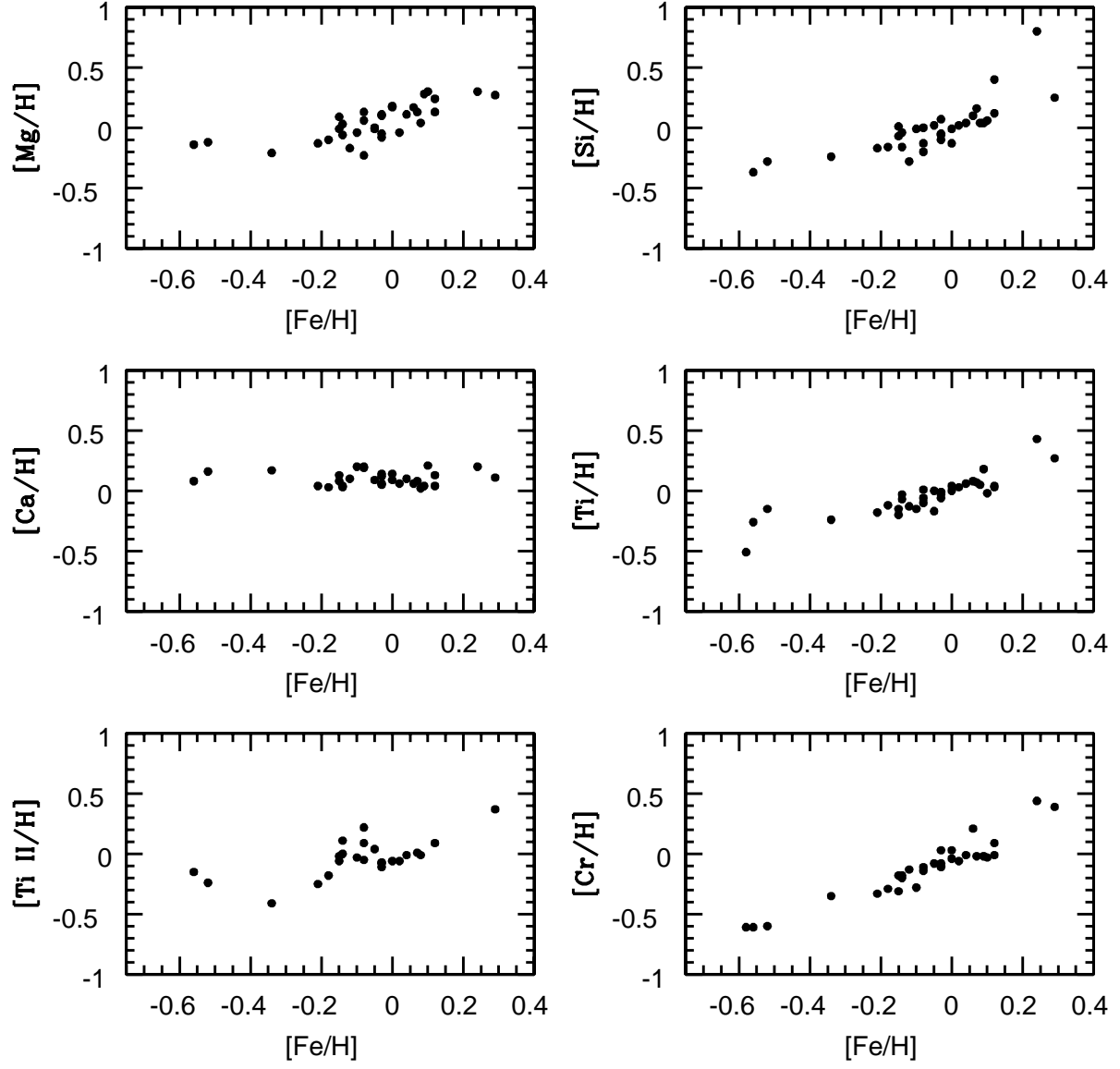


Fig. 15.— Abundance trends for all stars versus Fe/H.

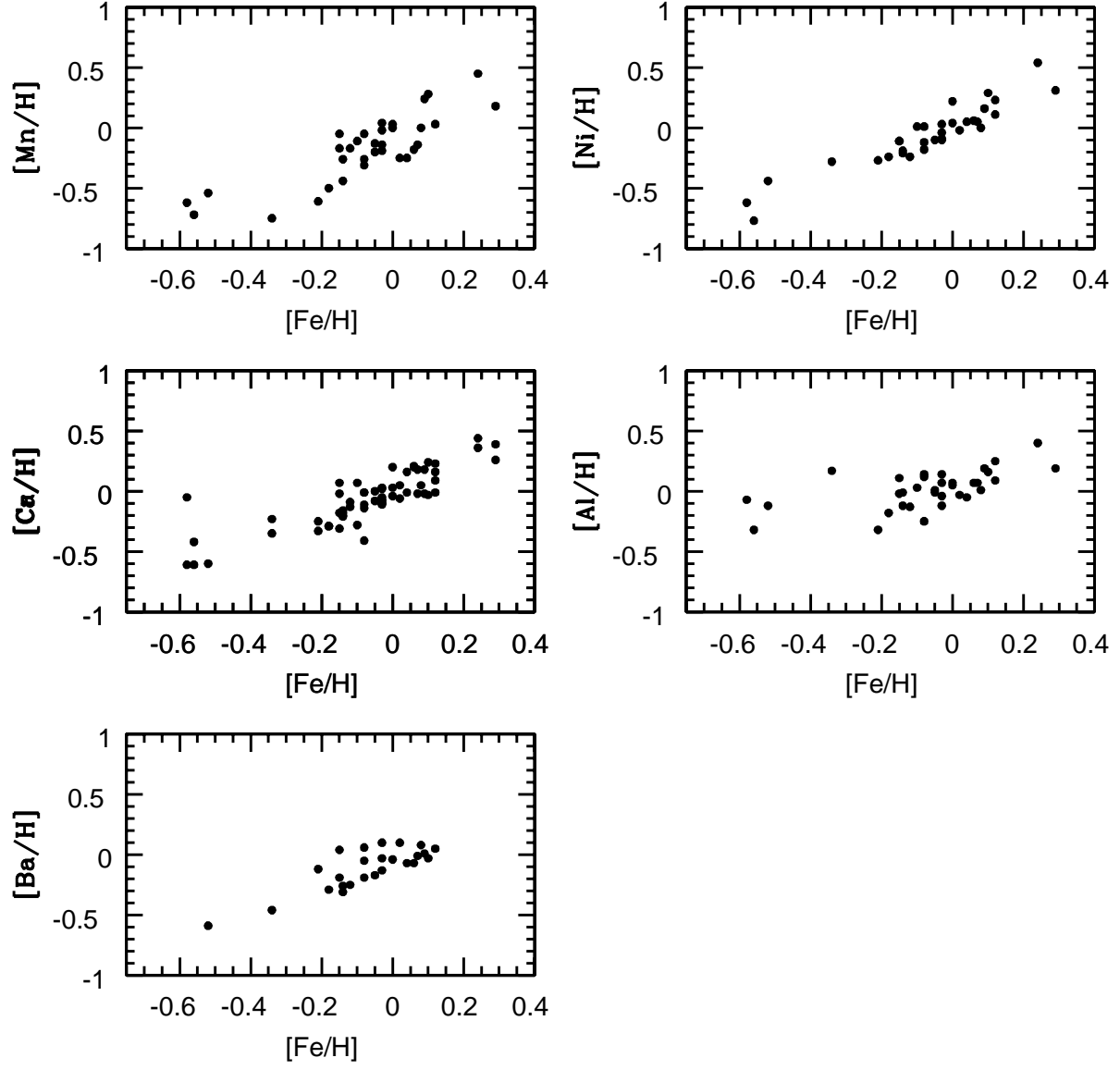


Fig. 16.— More abundance trends for all stars versus Fe/H .

